IN-CAT. 32
72100-CR

126 P.

JPL Publication 86-52

Geostationary Microwave Imagers

Detection Criteria

J.M. Stacey

December 15, 1986

National Aeronautics and
Space Administration

Jet Propulsion Laboratory
California Institute of Technology
Pasadena, California

JPL Publication 86-52

Geostationary Microwave Imagers

Detection Criteria

J.M. Stacey

December 15, 1986

National Aeronautics and
Space Administration

Jet Propulsion Laboratory
California Institute of Technology
Pasadena, California

The research described in this publication was carried out by the Jet Propulsion Laboratory, California Institute of Technology, under a contract with the National Aeronautics and Space Administration.

ABSTRACT

Geostationary orbit is investigated as a vantage point from which to sense remotely the surface features of the planet and its atmosphere--with microwave sensors. The geometrical relationships associated with geostationary altitude are developed to produce an efficient search pattern for the detection of emitting media and metal objects. Power transfer equations are derived from the roots of first principles and explain the expected values of the signal-to-clutter ratios for the detection of aircraft, ships, and buoys and for the detection of natural features where they are manifested as cold and warm eddies. The transport of microwave power is described for modeled detections where the direction of power flow is explained by the Zeroth and Second Laws of Thermodynamics. Mathematical expressions are derived that elucidate the detectability of natural emitting media and metal objects. Signal-to-clutter-ratio comparisons are drawn among detectable objects that show relative detectability with a thermodynamic sensor (microwave receiver) and with a short-pulse radar. These comparisons are modeled with identical antenna structures and at the same operating wavelength. Efficient and practicable antenna concepts are described as they apply to use in geostationary orbit.

FOREWORD

The advantages of operating microwave imagers and planetary surface-sensing equipment from geostationary orbit are abundant, and the rewards are many.

Nearly half of the surface of the planet is available at any instant of time for purposes of surveillance, scientific observation, and measurement. The expansive extent of the seas and land masses, including emitting objects and metal objects that are contained within them, are available for measurement, analysis, and the acquisition of data that is consigned for storage in the repositories and archives.

Microwave sensors are relatively invulnerable to the attenuating effects of the atmosphere, precipitation, and cloudforms; to this extent they are importantly advantaged over visible and infrared sensors. Given that microwave systems and sensors are endowed with sufficient capability, the extent of nearly a full hemisphere can be examined, at any time, for the occurrence of, and for the changes in, the populations of emitting objects and metal objects that are distributed over the surfaces of the seas and over the land mass. The microwave equipment needed to implement the observation of the planet is far more costly than the conventional equipment carried by planet-orbiting vehicles. But the cost is worth it in terms of the timely accessibility of information. The need to execute continuous observation of certain natural features and metal objects that are disposed on the surface of the sea and over the land is urgent, even crucial. The time of the observation is frequently of the essence. A large body of important, and needed, microwave observations of the planet can be executed, today, from geostationary orbit and with existing and state-of-the-art equipment.

It is time to implement the task. . . .

CONTENTS

Figures

Tables

SECTION 1
BACKGROUND

This monograph considers the practicability and application of microwave receivers when they are configured and construed as imaging systems that operate from geostationary orbit. Microwave imagers are perceived as multiwavelength sensors with articulating collecting apertures that efficiently scan the surface of the planet and view the

- Planetary atmosphere and the emissions from its gaseous and particulate constituents.

- Surface and its particular features thereon, including major sea, land, and ice masses.

- Emitting objects that are superposed upon the surface of the sea, exempli gratia, warm eddies, cold eddies, cold upwellings, major ocean currents, widespread storms, and hurricanes.

- Detectable metal objects, such as spacecraft, aircraft, ships, and moored buoys. Also included in the category of metal objects are land-based structures such as large antenna facilities and astronomical domes.

The term geostationary as it is embodied in the title of this monograph is construed to mean that the orbiting microwave imager maintains a constant orbital velocity and altitude and further that the position of the imager remains precisely fixed over a particular point on the rotating planetary surface in the equatorial plane. The imager is construed to be synchronized in both time and position to the rotation of the planet along the locus of the equator.

The terms geostationary and geosynchronous are used frequently and interchangeably in the contemporary technical literature. Because no well-defined or commonly understood distinction can be established between the two terms, they are regarded as synonymous.

The geometrical properties of geostationary orbit are very special, even unique. When a microwave imager is stationed precisely in geostationary orbit, the geometrical properties of the orbit cause the imager to remain stationary over a particular point on the locus of the equator, where its ground velocity is reckoned to be zero.

From the coign of vantage of geostationary orbit, the pointing axis of the collecting aperture for the microwave imager may be articulated in declination (north and south) in the plane of the meridian, where it moves along the meridian from pole to pole. Moreover, the pointing axis of the collecting aperture may be angularly displaced in longitude from the plane of the meridian, and in doing so, the pointing axis may view large surface areas on each side of the meridian, even to the horizon (sometimes called the limb of the planet). The horizon is perceived as a sharp physical boundary line that separates the solid surface of the planet from the Cosmic Background.

Three, or more, geostationary microwave imagers may be angularly disposed in position along the orbital path to gain coverage of the full areal extent of the planet, except for a small geographical area near the poles.

In comparison with the more conventional orbital altitudes for operational spacecraft and sensor systems, geostationary altitude is extremely high, id est, 35,760 kilometers to the plane of the meridian at the equator and 41,645 kilometers slant range to the limb. It is known that these large distances patently degrade the performance and the sensitivity of microwave sensors whose role it is to observe the surface of the planet and to resolve its features.

In the discussions that follow, we shall estimate critically the geostationary-orbit performance for several microwave sensors and draw comparisons among them. Mainly we shall determine which of the sensors are misapplications for geostationary orbit and which ones possess useful detection capabilities.

The performance capabilities of sensors operating at geostationary altitude are inextricably linked to the unique properties of the orbit-planet geometry. The large slant-ranges imposed by geostationary orbit limit sensor sensitivities and, moreover, require large collecting apertures. Pointing mechanisms and pointing controls require extraordinary stability.

SECTION 2

GEOMETRICAL PROPERTIES OF THE GEOSTATIONARY ORBIT AND THE PLANET

Geostationary spacecraft maintain a single, precisely fixed set of geographical coordinates (latitude and longitude) on the locus of the equator. The latitude coordinate is equal to zero and it lies in the plane of the meridian. The orbital location of the geostationary spacecraft, as referenced to the locus of the equator, can therefore be specified by longitude alone.

An elementary geometrical concept of a geostationary microwave imager, as it is perceived to point the axis of the conical-shaped antenna beam at a particular object on the equator, is illustrated in Figure 1. A more detailed view of geostationary relationships and geometry is given in Figure 2. Orbital and ground-track velocities and directions are indicated, and symbols are defined. Detailed geometrical properties of geostationary orbit are described quantitatively in Figure 3. Slant ranges and important angular relationships are defined and illustrated.

Geostationary microwave imagers can produce--at least in concept--an image of any particular surface area within the pale of the horizon.

From geostationary altitude, it is evident that even small angular movements of the pointing axis of the collecting aperture, especially as it moves toward the limb, produce large variations in the slant range to the surface (see Figures 1, 2, and 3).

The geostationary geometry is sometimes difficult to visualize because of the extreme sensitivities and interdependencies existing among key geometrical parameters, exempli gratia, nadiral angle, slant range, and latitude. Figure 4 and Table 1 elucidate the minutiae of geostationary geometry and provide a useful, insightful, and perspicacious understanding of its subtleties. Table 2 compares geostationary orbit with those at lower altitudes.

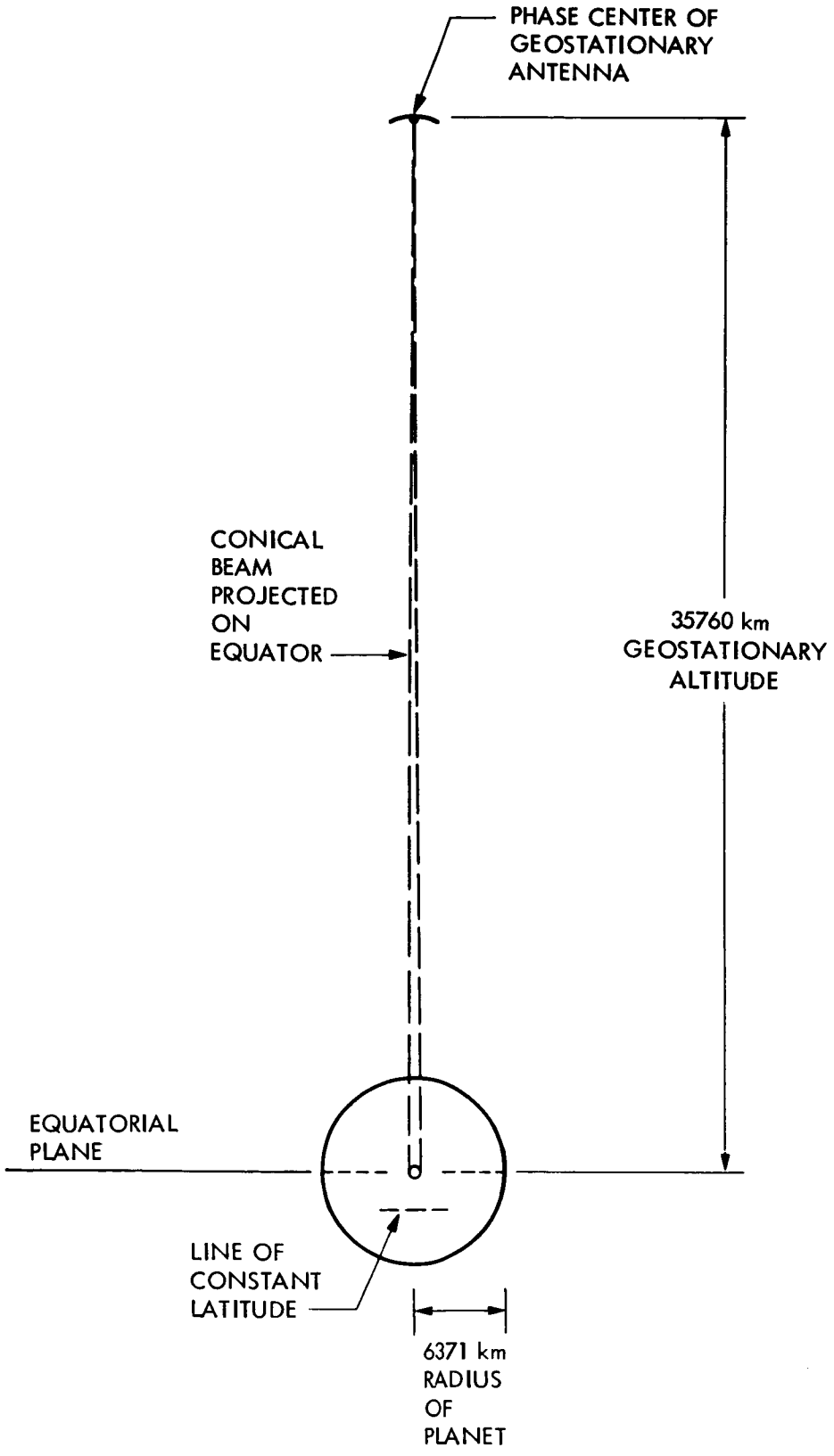

Figure 1. Elementary Geostationary Geometry

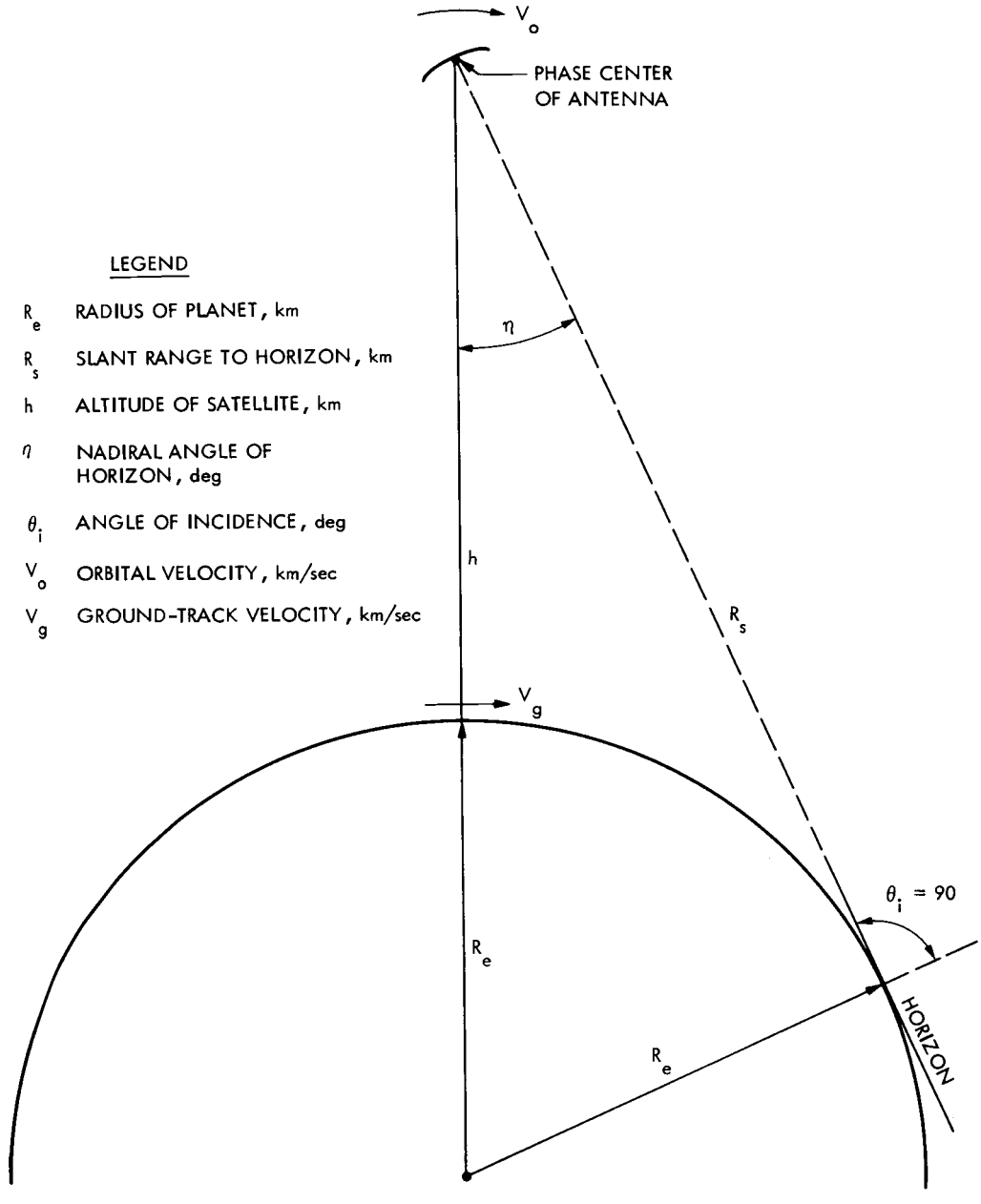

Figure 2. Geostationary Geometry With Symbol Definitions. The ground-track velocity, V_g, is synchronous with the rotation of the planet and so is equal to zero. The orbital velocity, V_O, is constant and numerically greater than zero. The slant range to the horizon (limb), R_S, shows that the horizon ray does not actually extend to the polar axis of the planet. The ray to the horizon is coincident with an angle of incidence, $\theta = 90$ degrees. The surface distance from $\theta_i = 90$ degrees to the pole (not shown) is 970 kilometers. The angle subtended by the surface distance to the pole, as referenced to the center of the planet, is 8.72 degrees. The surface distance represented by the subtended angle of 8.72 degrees is geometrically inaccessible to the sensor system on the spacecraft, except for its areal accessibility through the properties of microwave refraction in the troposphere.

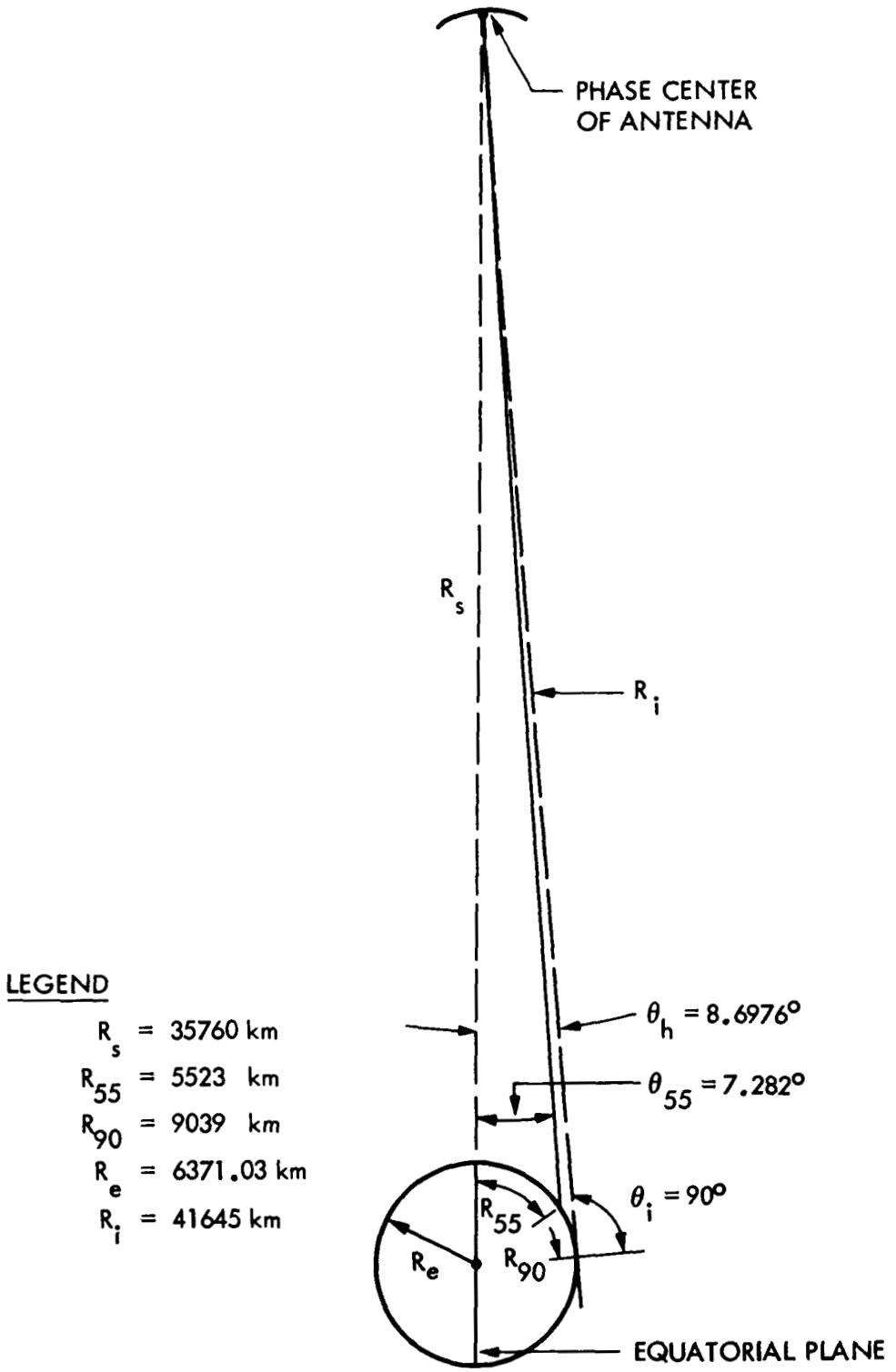

Figure 3. Detailed Geometrical Quantities of Geostationary Altitude. Nadiral angles, slant ranges, and arc-distances from the equator are given for approximately 55- and 90-degrees latitude, neglecting the 8.72-degree arc near the pole.

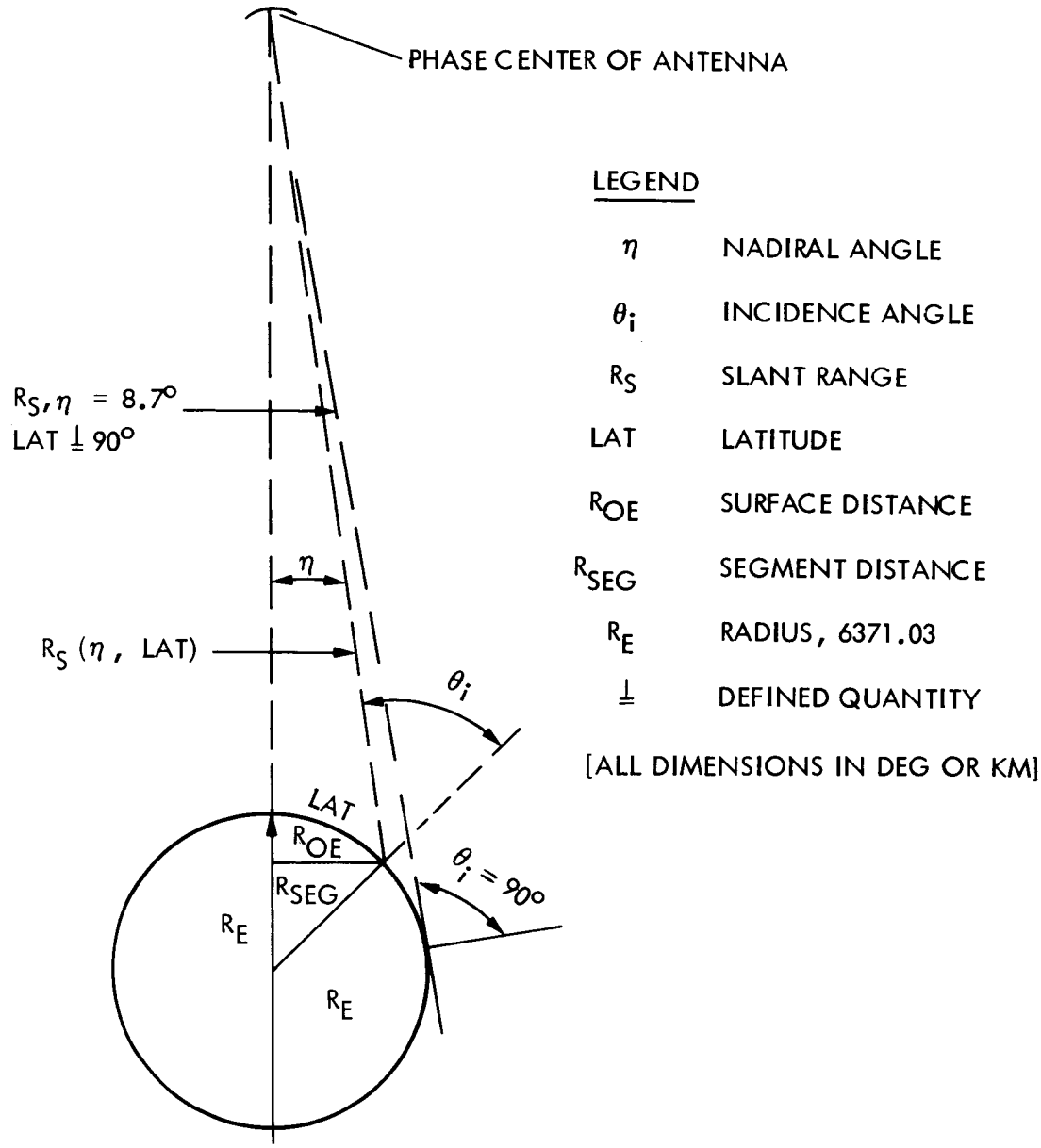

Figure 4. Planetary Geometry Affected by Geostationary Altitude

Table 1. Relevant Planetary Geometry Affecting Geostationary Altitude

LAT, DEG	η DEG	R_{OE} KM	R_{SEG} KM	R_S KM	θ_i DEG
0	0	0	0	35760	0
10	1.599	1005	1000	35853	10.6
20	3.135	2009	1976	36128	21.2
30	4.551	3013	2902	36575	31.6
40	5.80	4018	3757	37176	41.9
50	6.845	5022	4518	37909	52.0
60	7.663	6026	5167	38750	61.86
70	8.243	7030	5688	39670	71.46
80	8.586	8035	6069	40645	80.85
90	8.6976	9038	6297	41644	89.98

LEGEND

LAT	LATITUDE, DEG
η	NADIRAL ANGLE, DEG
R_{OE}	SURFACE DISTANCE, KM
R_{SEG}	SEGMENT DISTANCE, KM
R_E	RADIUS, 6371.03 KM
θ_i	INCIDENCE ANGLE, DEG

Table 2. Orbital Parameter Comparisons: Low-Altitude Orbits With Geostationary Orbits

h ALTITUDE, km	V_o ORBITAL VELOCITY, km/sec	V_g GROUND TRACK VELOCITY, km/sec	T ORBITAL PERIOD, hours	η NADIRAL ANGLE TO HORIZON, degrees	R_s SLANT RANGE TO HORIZON, km
250.00	7.76	7.00	1.49	74.20	1759
300.00	7.73	6.92	1.51	72.75	1950
350.00	7.70	6.84	1.52	71.43	2080
400.00	7.67	6.75	1.54	70.21	2232
450.00	7.64	6.68	1.56	69.07	2407
500.00	7.62	6.60	1.57	68.01	2510
600.00	7.56	6.45	1.61	66.05	2779
700.00	7.51	6.30	1.64	64.29	3051
790.00	7.46	6.17	1.68	62.83	3222
900.00	7.40	6.02	1.71	61.19	3418
954.00	7.38	5.95	1.73	60.43	3522
1000.00	7.35	5.89	1.75	59.81	3633
1334.00	7.19	5.48	1.87	55.78	4245
2000.00	6.90	4.79	2.12	49.56	5323
4000.00	6.20	3.34	2.92	37.90	8126
35760.00	3.08	0.00	24.00	8.70	41645

LEGEND:

R_e PLANET RADIUS, 6371.03 km

The proper interpretation of the calculated geometrical quantities given in this monograph is based upon the consideration that the planet is rotating from west to east with an equatorial rotational velocity of 0.4651 kilometers/second. The product of the universal gravitational constant, G, and the mass, M, is expressed as $GM = 3.98616 \times 10^5$ kilometers^3/second^2. The mean radius (6371.03 kilometers) is uniformly adopted for all geometrical computations in preference to the equatorial radius (6378.17 kilometers) [1].

The orbital parameters and calculated geometrical quantities that are expressed in the figures and tables are computed to the accuracy and precision needed for illustration purposes and for utilization in the examples that apply to microwave systems and microwave sensors. Other numerical values that are given for the radius of the planet or for the gravitational constant, for example, may produce slightly different results--the geometrical quantities shown in Tables 1 and 2 and in Figure 3 are cases in point. Investigators are encouraged to make their own individual computations of critical geostationary parameters where the ones given here may be lacking of sufficient accuracy.

SECTION 3

ARCHITECTURE OF A MICROWAVE IMAGE

The functional expectation of a geostationary microwave imager is to produce images of the planet and to detect certain features and objects thereon. The geostationary altitude is importantly advantaged: a large fraction of the planetary surface can be viewed at any time. The northern and southern hemispheres are equally visible except for a small area at the poles.

Given that surface features and object detections are feasible from geostationary altitude, let us proceed to discuss and illustrate the architecture of a particular microwave image that is especially adapted for the purpose. Later, we will calculate the expected value of the signal-to-noise (S/N) ratio for some selected objects both with a short-pulse radar and with a thermodynamic sensor[1,2]. For cases where the S/N is sufficiently large and positive, detection probabilities will also be calculated.

The architecture of microwave images requires some definitions for several new and needed terms. Terms of especial importance are: scene, instantaneous field of view (IFOV), field of view (FOV), and swath.[3]

The structure of a modeled microwave image is illustrated in Figure 5. The image pattern is constructed to show the geometrical projections of the principal lobe of an antenna whose collecting aperture is 730 meters[2]. The sensor (receiver) operates at 8-millimeters wavelength. The pointing axis of the antenna intercepts the meridian at 55-degrees north latitude.

The angular extent of the swath is given as 0.93 arc-degrees, which is the subtended angle as referenced to the phase-center of the antenna. The phase-center of the antenna contains an electrical impedance which is functionally construed as a point source.

The angular distance subtended by the swath is 1140 kilometers. The swath distance contains 100 IFOVs, each with a 30-millisecond dwell time. The total elapsed time for a swath is 3 seconds. The waveform that produces the swath is linear.

The diameter of each IFOV (scene), as it is projected on the surface, is 22.8 kilometers. The surface projection is based on the half-power antenna-gain level of the principal lobe of the antenna pattern. The angular extent of an IFOV is 0.0186 degrees, which is determined by the area of the collecting aperture at an operating wavelength of 8 millimeters. The IFOVs, shown in the line of the swaths, overlap at the 3-dB antenna-gain-level, the same as is shown for the overlapping IFOVs in the plane of the meridian. Greater separation among the IFOVs is purposely introduced into the image to reduce confusion as it is viewed by the eye.

The areal extent of the image is 1140^2 kilometers^2. The area is expressed by the product of the swath distance and the length of the conterminous IFOVs in the plane of the meridian.

The pattern of the IFOVs appears in their actual overlapped perspective in the plane of the meridian, id est, the IFOVs overlap at the 3-dB level of the antenna gain function. In the plane of the meridian, the overlapped swaths index northward from the equator. Within the angular extent of 0.9166 arc-degrees, the elapsed distance over the planet is 1140 kilometers. The 100 overlapped swaths that index northward in the plane of the meridian require 300 seconds of time.

Metal targets are identified in the image by small solid dots that are contained within the overlapped scenes. Actually, the metal targets (dots) appear within the overlapped regions of several scenes that occur in both the line of the swath and in the plane of the meridian. A metal target that is detected within the volume of the particular scene in one swath may be again detected in an adjacent overlapped swath 3 seconds later. Multiple and

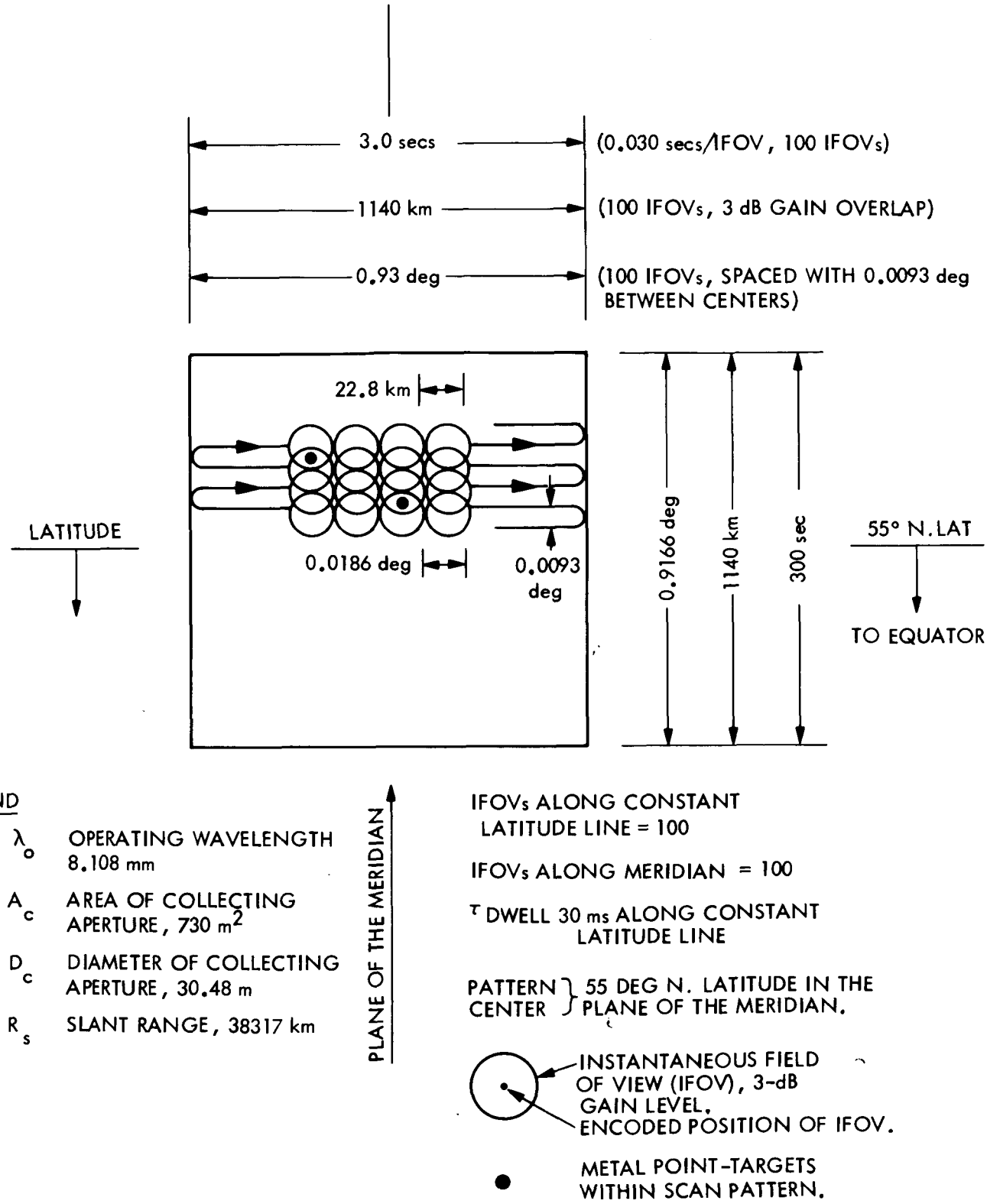

Figure 5. Morphology of a Microwave Image as It Is Viewed From Geostationary Altitude

redundant observations of the same metal target that occur within the same geographical area--and with a large time interval between observations--are highly decorrelated events that adumbrate high detection probabilities.

SECTION 4

DETECTION CRITERIA FROM GEOSTATIONARY ORBIT

In this section, we consider the detection criteria for both metal and emitting objects where they are construed as targets that are under a surveillance.

It seems fitting, and it is within the context of this monograph, to show the relative performance of sensors and their detection capability. By expectation, some sensors will fail because they are palpable misapplications from geostationary orbit; per contra, some succeed in a matter of degree.

The criterion for the success or failure of a sensor is reckoned, ultimately, by the magnitude of the signal-to-noise (S/N) or signal-to-clutter (S/C) ratio, whichever is appropriate. The S/N ratio is an excellent criterion to explain the performance of a microwave sensor system. A negative S/N ratio portends failure to detect. Large, positive S/N ratios are sine qua non for high confidence in the probability of detection.

In the operational use of many pulsed radar systems, the design specifications require a S/N ratio of +15 dB as a minimum value for all targets. In the radar community it has been determined empirically that a +15-dB S/N ratio produces good statistical confidence in a detection. In contrast, the signal component expressed by a +5-dB S/N barely exceeds the eye-observed noise level of the receiver, and the detection is only marginal, at best.

The S/N ratio is the most critical parameter that influences detection. It is also a necessary parameter for estimating detection probabilities.

In the discussion that follows, the detection capability of several geostationary microwave systems is determined for metal and emitting objects. A description of the associated microwave sensor is given and the S/N ratio is derived. Where it is interesting, useful, and appropriate, the probability of detection is calculated.

Considered also in this section are the modeled target-detection capabilities of a conventional short-pulse radar and a thermodynamic sensor (microwave receiver) while operating in geostationary orbit. Several other interesting categories of target detections are also analyzed.

Mainly, target detectability is modeled to show feasibility as it may occur in a matter of degree. Where a detection appears to be infeasible, the failure mechanisms are identified.

The short-pulse radar case is examined quantitatively for feasibility in the modeled case of an aircraft detection. The case is relevant and interesting: it is examined here mainly to show the mathematical terms that control the detectability of an aircraft target by an active geostationary sensor without regard for, or consideration of, its expectations of success.

An aircraft detection is also modeled for feasibility using a thermodynamic sensor (microwave receiver). The model is based on the transfer of microwave power from the impedance at the phase center of the antenna to the Cosmic Background through the intermediary bistatic-gain properties of the aircraft. It is shown that the transfer of microwave power--in this detection--is controlled by, and is consistent with, the Zeroth and Second Law of Thermodynamics.

Warm and cold eddies are perceived as laterally mobile graybody emitters (seawater medium) that are observed on the surface of the sea. The detectability of eddies is also examined, where the detection is influenced by their areal extent and by their temperature difference with respect to the surrounding seawater.

The microwave equipment that is used in these detection models operates at a wavelength of 8 millimeters. The antenna configurations that are used in the models are perceived as a symmetrical Cassegrain antenna for the short-pulse radar case and as an offset, prime-focus antenna for all

others. The collecting area for both antenna types contains 730 meters^2 or, equivalently, a paraboloid that is 30 meters in diameter.

The modeled cases for detection of metal objects and emitting objects include:

- Short-pulse radar observation of an aircraft. (See Appendix A.)
- Thermodynamic observation of the following metal objects over a sea background: an aircraft, buoy, and ship. (See Appendix B.)
- Thermodynamic observation of a cold eddy. (See Appendix C.)
- Thermodynamic observation of a warm eddy. (See Section 5.4.)

Epitomes of all modeled results are colocated in Section 5. Colocation is deliberate and purposeful because it is a convenient way to make performance comparisons among sensors and observed objects. The mathematical rationale for detection and the detailed system analyses are developed in the separate appendixes.

A matrix of detection capabilities, for all modeled cases, is given in Section 5.5.

SECTION 5

DETECTION-CAPABILITY COMPARISONS AMONG SENSORS

The comparative performance for several microwave sensor systems is modeled here where the sensors are perceived to operate from geostationary altitude. Detection capability is the critical consideration in this monograph, with the qualification that all sensor systems are endowed with the availability of the same microwave equipment and that all operate at the same wavelength.

A detailed analysis of the detection performance of each sensor is given in separate appendixes; the results of the analyses are colocated, discussed, and epitomized here.

A short-pulse radar system is chosen as one of the sensors to participate in the performance comparisons, knowing full well that it is significantly disadvantaged by the large slant ranges, especially those encountered at geostationary altitude.

It is well known in the radar art that the S/N ratio--the ultimate criterion for detectability--degrades by the fourth-power of the range. Nevertheless, radar-detection capability is interesting and informative at geostationary ranges--not necessarily from the standpoint of how well the radar succeeds in the detection, but rather how much extended capability is needed for it to succeed. The goals of the analyses are to detail the important loss terms that affect radar performance of a simple radar and to show, by example, how well the radar performs.

The basic radar equations are developed and organized from first principles, and the expression for S/N is derived and its terms are explained. The importance of each term is identified. The S/N ratio is the key parameter that affects detection--especially for threshold values. The probability of detection is computed from the S/N ratio, but only when it is numerically large and when the sign is positive.

In the analysis of the radar performance, several key expressions are produced whose terms explain the basic detection capabilities of the radar. The terms of the expressions are purposely structured to simplify performance extrapolations to radar systems that possess greater sophistication.

The analysis of the short-pulse radar is given in Appendix A. An epitome and an interpretive discussion of the radar capability are given in Section 5.1.

A thermodynamic sensor system is also modeled in the role of detecting a specified aircraft type from geostationary altitude. The term "thermodynamic sensor" is applied in these analyses to indicate that the sensor responds to microwave power that is produced by the radiant emittances and the irradiances of natural sources. A critically important segment of the performance analysis of the thermodynamic sensor system is to show how the sensor actually performs, how it operates, and how it is controlled by, and is consistent with, the fundamental laws of thermodynamics.

It is shown that the thermodynamic temperature of the impedance at the phase center of the antenna is in thermal equilibrium with the irradiance of the scene and that the condition of thermal equilibrium is controlled by the Zeroth Law of Thermodynamics. The sources and the magnitudes of the natural power sources are identified, and it is shown that the direction of the microwave power is controlled and guided by the Second Law of Thermodynamics.

The more descriptive and functional term "thermodynamic sensor" is adopted in this monograph in preference to "radiometer."

A thermodynamic sensor is perceived to operate in principle, by the equivalence of flux (microwave power) with thermodynamic temperature. Functionally, a thermodynamic sensor responds to the flux densities, radiant emittances, and irradiances of natural sources. It conforms to the principles of the Zeroth and the Second Laws of Thermodynamics which, in turn, explain the conditions of thermal equilibrium and determine the direction of the flow of microwave power.

The detection capabilities of a thermodynamic sensor are analyzed and discussed for an aircraft, buoy, and ship in Appendix B. The results of the analyses are epitomized and discussed in Section 5.2.

Also considered is the detectability of natural features on the sea surface as they are viewed from geostationary orbit. Natural features are manifested, in part, as warm eddies, cold eddies, upwellings, and major ocean currents. Natural features are also categorized as emitting objects because they possess thermometric and thermodynamic temperature differences with respect to the adjacent sea surfaces.

The modeled detection of a warm eddy is examined here where it is viewed from geostationary orbit. The detection is accomplished by employing the same equipment as the thermodynamic sensor and while operating at the same wavelength. A warm eddy (or current) is an excellent choice for the example because it exemplifies the character of the Gulf Stream in the Atlantic and the Kuroshio in the Pacific.

The power transfer equations that explain the emission from a cold eddy, as they are applied to a thermodynamic sensor, are derived in Appendix C. The signal-to-clutter (S/C) ratio for the detection of a warm eddy is computed and the results are epitomized and discussed in Section 5.4.

It is interesting and informative to investigate the power-transfer equations for a short-pulse radar and for a thermodynamic sensor where they are applied to the detection of a metal object (aircraft) and also of an emitting object such as a warm eddy. The structures of the mathematical terms are different for each case, but all conform to the conditions of thermal equilibrium and to the direction of power flow as is specified by the Zeroth and Second Laws of Thermodynamics.

5.1 SHORT-PULSE-RADAR DETECTION OF A CV-990/B-707 AIRCRAFT

The detailed analyses given in Appendix A for the short-pulse radar are epitomized here for purposes of consideration, comparison, and discussion.

Geostationary Geometry

Altitude	35,760 kilometers
Slant range to 55-degrees latitude	38,288 kilometers
Angle of incidence at 55-degrees latitude	57 degrees

Antenna Properties

Operating wavelength	0.008108 meters
Operating frequency	37 gigahertz
Antenna configuration	Symmetrical Cassegrain
Area of collecting aperture	730 meters^2
Diameter of the Cassegrain Paraboloid	30.48 meters
Gain (on-axis)	78.85 dB
Antenna efficiency	0.55

Receiver Properties

Predetection noise bandwidth	1.2 megahertz
Noise figure	5.0 dB (single-sideband)

Dissipative losses	3.0 dB
System noise temperature	4040 kelvins
Transmitter Properties	
Transmitter power	1000 watts (peak)
Transmitted waveform	1-microsecond pulse
Dissipative losses in transmit path	3 dB
Aircraft Properties	
Type	CV-990/B-707
Projected area of wing, fuselage, and tail sections from the perspective of normal incidence	382 meters^2
Backscattering coefficient	0.06 (-12.2 dBsm)
S/N (single-pulse)	-48.06 dB

The single-pulse S/N is computed to be -48.06 dB for the CV-990/B-707 aircraft as it is viewed topside from an incidence angle of 57 degrees and while it maintains level flight at 55 degrees latitude. The sign of the S/N ratio is negative--and large. For these reasons alone, detection capability fails.

By expectation then, a short-pulse radar will fail to detect a CV-990/B-707 aircraft from geostationary orbit. The radar analyses examine the individual factors that limit radar performance and show the results. From these analyses, it is no surprise that the fourth-power exponent of the slant range is the principal limiting factor, as is clearly shown in Equation (A-6).

It has been firmly established by operating experience, and amply confirmed with applied statistics and probability models, that large S/N ratios must exist if a measured radar parameter is to be estimated with good accuracy or precision. From this, and as a matter of practice, radar systems designers typically size the equipment performance to produce a minimum S/N ratio of +15 dB for a specified backscattering cross-section.

Given that the +15 dB detection criterion is applied to the -48 dB single-pulse S/N ratio shown in the model, the radar designer must improve the system performance of the radar by 63 dB. To realize a system performance improvement of this magnitude, only the transmitter power, collecting aperture area, and receiver noise temperature are available.

5.2 DETECTION MODEL OF AN AIRCRAFT, BUOY, AND SHIP

5.2.1 Detection of a CV-990/B-707 Aircraft With a Thermodynamic Sensor

The detailed analyses given in Appendix B for the detection of a CV-990/B-707 aircraft with a thermodynamic sensor are epitomized here for purposes of comparison and discussion.

Geostationary Geometry

Altitude	35,760 kilometers
Slant range to 55-degrees latitude	38,288 kilometers
Angle of incidence at 55-degrees latitude	57 degrees

Antenna Properties

Operating wavelength	0.008108 meters
Operating frequency	37 gigahertz
Antenna configuration	Offset, prime-focus
Area of collecting aperture	730 meters^2
Diameter of the offset, prime-focus paraboloid	30.48 meters
Gain (on-axis)	78.85 dB
Solid-angle main-beam efficiency	0.95

Receiver Properties

Predetection noise bandwidth	100 megahertz

Temperature resolution (S/N = 1)	1 kelvin
Sea Background Properties	
Mean thermodynamic temperature of the sea scene (which is also the thermodynamic temperature of the impedance at the phase center of the antenna) [from Figure A-4]	129 kelvins
Blackbody temperature of the Cosmic Background	2.7 kelvins
Clutter temperature (thermodynamic) [estimated from References [3]and [5]]	0.45 kelvins
Orthogonal average (root sum of squares) of the temperature resolution and the clutter temperature	1.1 kelvins
Metal-Object Properties	
Aircraft type	CV-990/B-707
Projected area of aircraft at normal incidence, with projected area contributions from the wing, fuselage, and tail sections	382 meters^2
Bistatic scattering coefficient	0.06 (-12.2 dBsm)
$\underline{\hat{S}}$ C, the expected value of the S/C ratio	24.61, or +13.91 dB

False alarm time [from Figure 5]	60 seconds
Probability of false alarm [referenced to Figure 5]	4×10^{-4}
Probability of detection [referenced to Figure 5]	0.74 or 74%

The computations of the $\frac{S}{C}$ ratio and the probability of detection are based on the solutions of expressions (B-8) and (B-9). The modeled quantities are estimated for a CV-990/B-707 type of aircraft that is in level flight and is superposed upon a sea background. The aircraft is disposed in altitude above the attenuating atmosphere of the planet.

The detection is powered by the irradiances and radiant emittances of natural sources. In this model, the impedance at the phase center of the antenna, Z_{pc}, is in thermal equilibrium with the scene. Thermal equilibrium is maintained between the scene and Z_{pc} by the principle of reciprocity in the antenna gain function.

The available power for the detection of the aircraft is deduced from the difference between the thermodynamic temperature of the scene and the blackbody temperature of the Cosmic Background. The bistatic scattering properties of the aircraft operate to redirect the incident power from the phase center of the antenna to the Cosmic Background. The bistatic properties of the aircraft are produced by the Kirchhoff-Huygens Principle of reradiation from metal objects.

The terms of expression (B-5) explain the detection criteria for the aircraft.

The expected value of the S/C ratio is computed to be +13.9 dB, which is based on the geometrical parameters of the geostationary geometry and on relevant electrical properties of the aircraft and the collecting aperture of the antenna.

The antenna and the observing equipment, as they are defined in the model, are reasoned to be feasible and in most cases they are known to be state of the art.

It is evident from the terms of (B-5) that the apparent projected area of the aircraft--and correspondingly, the S/C ratio--will increase at lower latitudes. Also at lower latitudes, slant range decreases near the equator, where it approaches the limiting value of geostationary altitude.

The angle of incidence, θ_i, modifies the magnitude of the projected area of the aircraft; in fact, the projected area of the aircraft varies as (cosine θ_i)^2. At low latitudes, the angle of incidence approaches zero. (See Figure 2.)

In a performance comparison using basically the same equipment and using the same aircraft target, the short-pulse radar fails the detection with a -48 dB S/N ratio and the thermodynamic sensor succeeds with a +13 dB S/C ratio.

The conclusions of the analysis of the thermodynamic sensor augur that aircraft types with larger projected area than the CV-990/B-707 will produce larger S/C ratios and correspondingly larger probabilities of detection. By expectation, smaller aircraft will produce smaller, but perhaps still useful, S/C ratios.

5.2.2 Detection of a Metal Buoy

5.2.2.1 Metal Buoy at 55 Degrees Latitude. The detailed model of the 12-meter-diameter metal buoy that is positioned in the plane of the meridian at 55 degrees latitude is analyzed in Appendix B immediately following the detection analysis for the CV-990/B-707 type of aircraft. The assumptions given in the model and the observing equipment on the satellite are excerpted from Appendix B and are epitomized here.

Immediately following this section, in Section 5.2.2.2, is the epitome for the 12-meter-diameter metal buoy where it is positioned at the equator in the plane of the meridian of the satellite. This colocation technique ensures that comparisons between the two buoy locations are readily accessed.

Geostationary Geometry for the Metal Buoy

Altitude	35,760 kilometers
Slant range to 55-degrees latitude	38,288 kilometers
Angle of incidence at 55-degrees latitude	57 degrees

Antenna Properties

Operating wavelength	0.008108 meters
Operating frequency	37 gigahertz
Antenna configuration	Offset, prime-focus
Area of collecting aperture	730 meters^2
Diameter of the offset, prime-focus paraboloid	30.48 meters

Gain (on-axis)	78.85 dB
Solid-angle main-beam efficiency	0.95
Receiver Properties	
Predetection noise bandwidth	100 megahertz
Temperature resolution (S/N = 1)	1 kelvin
Sea Background Properties	
Mean thermodynamic temperature of the sea scene (which is also the thermodynamic temperature of the impedance at the phase center of the antenna) [from Figure A-4]	129 kelvins
Blackbody temperature of the Cosmic Background	2.7 kelvins
Clutter temperature (thermodynamic) [estimated from References [3] and [5]]	0.45 kelvins
Orthogonal average (root sum of squares) of the temperature resolution and the clutter temperature	1.1 kelvins
Metal-Object Properties	
Buoy type	Discus
Diameter	12 meters

Projected area at normal incidence	113.1 meters^2
Bistatic scattering coefficient	0.06 (-12 dBsm)
$\hat{\frac{S}{C}}$, the expected value of the S/C ratio	1.92 dB

The solution to Equation (B-8) for the expected value of the S/C ratio for a 12-meter-diameter buoy at 55 degrees latitude yields a numerical value of 1.55 or 1.92 dB. Because of the low numerical result given by the S/C ratio, the detection is regarded as a threshold case. Again, we are informed that the solution to Equation (B-8), and the detection statistics thereof, are keyed to the search and model given in Figure 5.

It is interesting, but of little value, to compute the probability of detection of the buoy based on the computed value of the S/C ratio. Actually, the probability of detection is 0.05 based on a false alarm rate of 4×10^{-4} and on a S/C ratio of 1.55, which portends the expectation that less than 1 buoy out of an ensemble of 10 will be detected at 55 degrees latitude.

5.2.2.2 Metal Buoy at the Equator and in the Nadiral Path of the Geostationary Satellite. By expectation the S/C ratio for the buoy will improve when the buoy is located on the equator and in plane of the meridian (the nadiral path of the geostationary satellite). The improvement in the S/C ratio at the equator is occasioned by

- o Shorter slant range.
- o Larger projected area because the cosine of the incidence angle reduces to 1 in Equation (B-8).
- o Path lengths through the atmosphere are shorter at the zenith rather than in the slant paths to 55 degrees latitude.

To this extent we modify the terms of Equation (B-8) to show

R_s = Slant range: $35{,}760 \times 10^3$ meters (from $38{,}288 \times 10^3$ meters).

T'_{CB} = Thermodynamic temperature of the Cosmic Background as affected by the transmission paths through the atmosphere: 31 kelvins (from 38 kelvins).

θ_i = Angle of incidence: 0 degrees (from 57 degrees).

All other terms in Equation (B-8) for the buoy at 55 degrees latitude remain unchanged.

By substituting the changed values for R_s, T'_{CB}, and θ_i in Equation (B-8), we obtain

$$\frac{\hat{S}}{C} = 6.37 \text{ as a numeric quantity, or } 8.04 \text{ dB}$$

From the solution of Equation (B-9), for the probability of detection, given that the false alarm rate is 4×10^{-4} and that the search model is defined by Figure 5,

$$P_d = (4 \times 10^{-4})^{[1/(1 + 6.37)]}$$

$$= 0.35$$

which is interpreted to mean that 3 buoys out of 10 are expected to be detected by the search pattern expressed in Figure 5 when the buoys are located in the nadiral path of the geostationary satellite at the equator.

5.2.3 S/C Ratio and Probability of Detection of an Aircraft Carrier

The detailed analysis given in Appendix B for the detection of the U.S.S. Columbia class aircraft carrier is epitomized here for purposes of comparison and discussion.

Geostationary Geometry

Altitude	35,760 kilometers
Slant range to 55-degrees latitude	38,288 kilometers
Angle of incidence at 55-degrees latitude	57 degrees

Antenna Properties

Operating wavelength	0.008108 meters
Operating frequency	37 gigahertz
Antenna configuration	Offset, prime-focus
Area of collecting aperture	730 meters^2
Diameter of the offset, prime-focus paraboloid	30.48 meters
Gain (on-axis)	78.85 dB
Solid-angle main-beam efficiency	0.95

Receiver Properties

Predetection noise bandwidth	100 megahertz
Temperature resolution (S/N = 1)	1 kelvin

Sea Background Properties

Mean thermodynamic temperature of the sea scene (which is also the thermodynamic temperature of the impedance at the phase center of the antenna) [from Figure A-4]	129 kelvins
Blackbody temperature of the Cosmic Background	2.7 kelvins
Clutter temperature (thermodynamic) [estimated from [3] and [5]]	0.45 kelvins (1-σ)
Orthogonal average (root sum of squares) of the temperature resolution and the clutter temperature	1.1 kelvins

Metal-Object Properties

Aircraft carrier type	U.S.S. Columbia class
Projected area of aircraft carrier at normal incidence, based on a nominal length of 329 meters and a width of 82 meters	26,978 meters^2
Bistatic scattering coefficient	0.06 (-12 dBsm)

The solution to equation (B-8), in Appendix B for the expected value of the S/C ratio on a clear day yields a numerical value of 88,443, or 49.5 as a decibel (dB) ratio.

The probability of detection is calculated from equation (B-9) from the search model at 55 degrees latitude as shown in Figure 5. For a false alarm that exceeds the detector threshold every 60 seconds,

$$P_N = 4 \times 10^{-4}$$

and the probability of detection is expressed by substitution in equation (B-9),

$$P_d = (4 \times 10^{-4})[1/(1+88,443.16)]$$

$$= >0.99$$

It is not surprising that the aircraft carrier of the U.S.S Columbia class produces such a large S/C ratio, even at 55 degrees latitude. The rectangular prism figure of the aircraft produces a large forward-scattered lobe in the direction of the zenith by the Kirchhoff-Huygens Principle of reradiation. The expansive deck structure is mainly metal. Certain areas of the deck are reasoned to be relatively smooth on the scale of 8-millimeters wavelength, which will increase the forward-scattered gain. As a casual point of commentary, the projected area of the deck at normal incidence exceeds 6.5 acres. Moreover, because the surface of the deck is relatively flat, and has a regular geometry, the assumed bistatic scattering coefficient (0.06) may be too low.

5.3 DETECTION OF A COLD EDDY WITH A THERMODYNAMIC SENSOR

The sea surfaces of the planet continually show the occurrences of cold areas that are formed by cold ocean currents. Sometimes the cold areas that are manifested on the surface are produced by cold currents that move along the bottom of the ocean and are deflected to the surface by physical obstructions. Sometimes cold spots are produced by major ocean currents such as the Gulf Stream or the Kuroshio.

The system of circulating seawater that flows around the Antarctic Continent produces a system of capricious streams of cold Antarctic seawater that submerges below the warmer water to the north and later reemerges on the surface at very low latitudes--even as far north as the equatorial belt.

Cold areas are variously called "cold rings," "cold spots," or "cold upwellings," depending upon the oceanographic mechanism that produces them and upon the locality where they are known to occur. Manifestations of localized cold areas on the surface of the sea are important because they infer circulation patterns and the distribution of seawater at different temperatures.

Thermodynamic sensors on geostationary satellites detect cold areas on the sea surface with good S/C ratios. From this capability, significant contributions are made to the discipline embraced by oceanography.

The detectability of cold eddies is modeled in Appendix C. Expressions are derived for the expected value of the S/C ratio as a function of the latitude where they occur on the planet. From the analysis it was determined that a cold eddy with a circular figure that is 50 kilometers in diameter could be detected

- At 55 degrees latitude with a S/C ratio of 15.37 dB.
- At the equator, in the plane of the meridian, with a S/C ratio of 28.4 dB.

The detectability of the cold eddy is based on the search model explained by Figure 5 and as computed by Equation (C-3), which is derived in Appendix C. The solution to Equation (C-3) is based on the following modelled assumptions:

Operating wavelength of the thermodynamic sensor	0.008108 meters (37 gigahertz)
Altitude of the geostationary-borne thermodynamic sensor	35,760 kilometers
Slant range to 55 degrees latitude	38,288 kilometers
Collecting area of the antenna (30.48 meters diameter)	730 meters^2
Solid-angle main-beam efficiency of collecting aperture	0.95
Orthogonal average of the temperature resolution of the receiver (1 kelvin) and the thermodynamic temperature of the clutter (0.45 kelvins)	1.1 kelvins
Thermodynamic temperature of the scene [from Figures A-3 and A-4]	128.87 kelvins
Emissivity of the seawater within the scene	0.35
Thermometric temperature of the propagation path from the phase center of the antenna to the Cosmic Background and including the thermodynamic properties of the surface of the cold eddy [see Equation (C-4) in Appendix C]	123.94 kelvins

Emissivity of the seawater at the smooth surface of the cold eddy at an incidence angle of 57 degrees	0.2
Thermometric temperature difference between the surfaces of the cold eddy and the adjacent seawater	2 kelvins

From the entries of the modeled quantities into the terms of Equation (C-3) in Appendix C, the expected value of the S/C ratio is computed for a cold eddy at 55 degrees latitude is:

$$\hat{\frac{S}{C}} = 15.37 \text{ dB}$$

and for the same 50-kilometer-diameter cold eddy on the equator:

$$\hat{\frac{S}{C}} = 28.4 \text{ dB}$$

These S/C ratios are reasoned to be sufficiently large to produce good detection capability of the cold eddy either at 55 degrees latitude or at the equator.

5.4 DETECTION OF A WARM OBJECT WITH A THERMODYNAMIC SENSOR

By expectation, and from experience, remote sensing of the sea surface from geostationary orbit will reveal patterns of warm objects that are disposed upon the surface of the sea.

The bores of certain warm ocean currents, such as the Gulf Stream and the Kuroshio, produce congeries of warm objects along their sides as they thrust through the sea. Frequently, when the meandering bore of the Gulf Stream passes through the northern perimeter of the Sargasso Sea, warm water from the Sargasso Sea is pinched off and abandoned as a warm eddy. When the eddy passes near, or through, the cold Labrador Current that flows southwestward along the coast of North America, the eddy is clearly manifested as an isolated and conspicuous mass of warm seawater.

The natural circulation patterns of the sea and its currents continually operate in consonance to produce an ever-changing pattern of warm seawater objects.

Warm, emitting objects sometimes occur on the surface of the sea that have manmade origins. Cases in point include: oil spills and oil discharges from ships, mud from underwater mining activities, and a host of floating pollutants.

The term warm, where it is construed as referring to an object that is detectable with microwave sensors, means that the object is warm with respect to the integrated thermodynamic temperatures of the atmosphere and the sea that is contained within the principal lobe of the antenna pattern, id est, within the volume of the scene.

The mathematical expressions that explain the transfer of microwave power from natural emitters on the sea surface to the collecting apertures of microwave sensors in orbit are different for cold and warm bodies. That is, the transport of microwave power is in opposite directions, to be consistent with the Second Law of Thermodynamics. Appendix C shows the development of expressions that explain the detectability of cold objects on the sea.

Reference [4] details the development of the mathematical expressions that explain the detectability of warm objects.

Reference [6] reviews the fundamental concepts, principles, and mathematical expressions that show the transfer of microwave power from a warm object on the sea surface to the impedance at the phase center of a collecting aperture in orbit. It is shown that the radiant emittance of a warm emitting object is explained by the Stephan-Boltzmann equation. From the Stephan-Boltzmann equation, the radiant emittance of a warm object of is given by:

$$W' = \varepsilon \sigma T^4, \text{ in watts/meter}^2$$

where

ε = The emissivity of the warm emitting surface, a dimensionless quantity.

$\sigma = 5.67032 \times 10^{-8}$, in watts/meter^2 K^4, the Stephan-Boltzmann constant.

T = Difference in temperature existing between the blackbody temperature of the emitting object and the surrounding seawater medium.

The symbol T is construed to be the temperature of a blackbody or a graybody. By definition, the emissivity of a blackbody is equal to 1. For a graybody, the emissivity is less than 1, but it is constant.

For the cold eddy, the available microwave power is proportional to the linear difference in temperature between the cold eddy and the surrounding surface media. For a warm eddy, the available microwave power is proportional to T^4.

From Reference [6], Equation (11c), the closed-form equation is adopted that explains the transfer of microwave power from a warm object on the sea to the electrical impedance at the phase center of a collecting aperture in orbit.

We rewrite Equation (11c) as given in [6] for use in this monograph as follows:

$$\frac{S}{C} = \frac{(2.57 \times 10^{14})\ \varepsilon\ T^{4}\ (\cos \theta_i)\ \ell^{2}\ (A_c \eta)}{R_s^{2}\ T'\ B_n\ \ell_{au}} \qquad (5.4\text{-}1)$$

where

ε = Emissivity, a dimensionless quantity.

T = Difference in temperature between the warm eddy and the surrounding sea media, in kelvins.

θ_i = Incidence angle, in degrees.

A_c = Area of the collecting aperture, in meters^2.

η = Solid-angle main-beam efficiency of the antenna, a dimensionless quantity.

R_s = Slant range, in kilometers.

T' = Orthogonal average of the temperature resolution (1 kelvin) of the receiver with the clutter temperature (0.45 kelvins).

ℓ = Circular diameter of a warm eddy where it is perceived as a Lambertian disk emitter, in meters.

B_n = Predetection bandwidth of the receiver, in hertz.

ℓ_{au} = Loss in the atmospheric path from the warm eddy to the impedance at the phase center of the antenna. This loss term is expressed as a number greater than 1.

The terms of equation (5.4-1) do not show the operating wavelength (λ = 8 millimeters) explicitly because the radiant emittance of the source is construed as blackbody or graybody radiation. In practice, the predetection bandwidth of the receiver, B_n, is centered at the operating wavelength of the antenna.

By substitution in the terms of equation (5.4-1) for the modeled detection of a warm eddy, where the eddy is construed to be a Lambertian disk emitter, at 55 degrees latitude and where the detection is based on the search model described in Figure 5, we get the following:

$\epsilon = 0.35$

$\theta_i = 57$ degrees

$T = 1.5$ kelvins

$\ell = 5000$ meters

$A_c = 730$ meters^2

$\eta = 0.95$

$R_s = 38{,}288 \times 10^3$ meters

$T' = 1.1$ kelvins

$B_n = 10^8$ hertz

$\ell_{au} = 1.08$ (0.35 dB)

$$\frac{S}{C} = \frac{(2.57 \times 10^{14})\ (0.35)\ (1.5)^4\ (\cos 57)\ (5000)^2\ [(730)(0.95)]}{(38{,}288 \times 10^3)^2\ (1.1)\ (10^8)\ (1.08)}$$

$= 24.69$, or 13.93 dB

To estimate the S/C ratio at the equator and in the plane of the meridian, the following substitutions are made:

- R_s = 35,760 x 10^3 meters. The slant range and the altitude are identical parameters on the equator and in the plane of the meridian.

- The angle of incidence is changed from 57 degrees to θ_i = 0 degrees.

- The attenuation through the zenith path, as versus the long slant path through the atmosphere at 55 degrees latitude, reduces to 0.2 dB (1.047, a number greater than 1), so ℓ_{au} = 1.047 (0.2 dB).

By substitution in the terms of equation (5.4-1) for the equatorial detection of the warm eddy, we obtain

$$\frac{S}{C} = 53.61, \text{ or } 17.29 \text{ dB}$$

Notably the S/C ratio increases from 13.93 dB at 55 degrees latitude to 17.29 dB at the equator in the plane of the meridian.

5.5 MATRIX OF DETECTION CAPABILITY

An overview of the detection capabilities of the metal and emitting objects that are considered in this monograph is given in matrix form in Table 3. The geostationary equipment for all sensors are basically the same: a paraboloid, whose diameter is 30.48 meters. The atmospheric conditions are expressed by a clear day both at 55 degrees latitude and at the equator. All sensors share a common operating wavelength: 8 millimeters.

Table 3. Summary of Detection Capability From Geostationary Orbit

Object	Sensor	Latitude, degrees	S/C, dB	P_d
Aircraft CV-990/B-707	Short-pulse radar	55	-48	--
Aircraft CV-990/B-707	Thermodynamic	55	13.9	0.74
Metal Buoy (12-meter diameter)	Thermodynamic	55	1.9	0.05
Metal Buoy (12-meter diameter)	Thermodynamic	0	8.0	0.35
Aircraft Carrier (U.S.S. Constellation class)	Thermodynamic	55	49.5	>0.99
Cold Eddy (50-kilometer diameter)	Thermodynamic	55	15.4	--
Cold Eddy (50-kilometer diameter)	Thermodynamic	0 (Equator)	28.4	--
Warm Eddy (5-kilometer diameter)	Thermodynamic	55	13.93	--
Warm Eddy (5-kilometer diameter)	Thermodynamic	0 (Equator)	17.29	--

The sensor identification column introduces the term "thermodynamic." This term is purposefully coined in this monograph to convey more clearly the concept that a microwave receiver operates by the instantaneous equivalence of microwave power and thermodynamic temperature as it is manifested either in free space as a wavefront or in a contained medium such as a waveguide.

When the thermodynamic connotation is applied to a microwave system, the direction of propagation is construed to be controlled by the Laws of Thermodynamics, principally the Zeroth and Second laws.

The detection models use two latitudes: 55 degrees and 0 degrees (the equator). The rationale for 55 degrees latitude is that many interesting and important observable and detectable objects lie within a wide belt near 55 degrees. At 55 degrees latitude, however, the projected areas of the observed objects are diminished by the cosine of the incidence angle. At the equator, the incidence angle is zero. The detectivity of an object is enhanced at the equator because the slant range reduces to the altitude of the satellite. The slant range from the satellite to an object on the equator is significantly shorter than the slant range to 55 degrees latitude.

The probability of detection is computed from the S/C ratio for each object and the false alarm rate as given by the search pattern in Figure 5. Basically, the false alarm rate allows the threshold setting of the detector to be exceeded once in every 60-second period.

The interpretation of the probability of detection, P_n, is reckoned to be analogous to the familiar blip-scan-ratio as it is applied in radar detection for a PPI display. That is, a 0.74 probability of detection is construed to mean that 7 out of 10 objects, each with the same signal statistics, will be detected by the thresholded detector over the extent of the search pattern (Figure 5).

SECTION 6
THE GEOSTATIONARY PERSPECTIVE

Doubt, curiosity, and serendipity are like fertile seeds: they sprout, mature, and produce--knowledge.

The view of the planet from a point in geostationary orbit, and from the perspective of a microwave imager, amply elucidates the importance of the geostationary altitude as the ultimate vantage point for remotely sensing the properties of the planetary atmosphere, its expansive seas, and its land masses.

From any one point in geostationary orbit, the planetary scene extends to high latitudes at the poles and to nearly the total diameter of the planet at the equator. The solid angle subtended by the planet from geostationary altitude is 0.0723 steradians. The polar regions and the limb of the planet near the equator are not directly observable except by the processes of atmospheric refraction. The plane angle subtended by the limbs of the planet, at the equator, is 17.4 degrees. The coign of vantage of a point in geostationary orbit features a view of space over a solid angle of $4-\pi$ steradians.

A view of the planet, with some of its celestial companions, is illustrated in Figure 6. Table 4 summarizes, by categories, some of the illustrated features.

Geostationary observations require high-performance microwave equipment and sensors. The mechanical and electrical designs of the antenna, for example, are critical considerations. Extremely high antenna gain must be achieved at the operating wavelength. High antenna gain is accomplished by large collecting apertures, high antenna efficiencies (solid-angle main-beam efficiency) and short operating wavelengths.

Figure 6. Remote Sensing Perspective From Geostationary Altitude

Table 4. Background Related Objects

Backgrounds		
Land	Sea	Cosmic
Warm Objects	**Warm Objects**	**Warm Objects**
o Deserts	o Warm Currents	o Sun
o Rain Forests	o Warm Eddies	o Moon
		o Planets
Cold Objects	**Cold Objects**	
o Lakes	o Eddies	
o Rivers	o Upwellings	
o Iceforms	o Currents	
Metal Objects	**Metal Objects**	**Metal Objects**
o Spacecraft	o Spacecraft	o Spacecraft
o Aircraft	o Aircraft	o Manmade Objects
o Antennas	o Ships	
o Astrodomes	o Buoys	
Volume Emitters	**Volume Emitters**	**Volume Emitters**
o Cloudforms	o Cloudforms	o Space Gases
o Rain	o Rain	
o Atmospheric Gases	o Atmospheric Gases	

An adaptable antenna design to implement efficient planetary observations from geostationary orbit is illustrated in Figure 7. The antenna configuration is an offset, prime-focus one. The contour accuracy (1/32 of a wavelength) of the primary reflector, with respect to a theoretical paraboloid, is 253 micrometers (0.010 inches), which is consistent with high-gain operation at 8-millimeters wavelength. The diameter of the collecting aperture is scalable, as the need requires. The detection models that are developed in this monograph use, as a common basis for comparison, a 30.34-meter-diameter aperture, which is reasoned to be practicable for geostationary deployment and it is known to be state of the art.

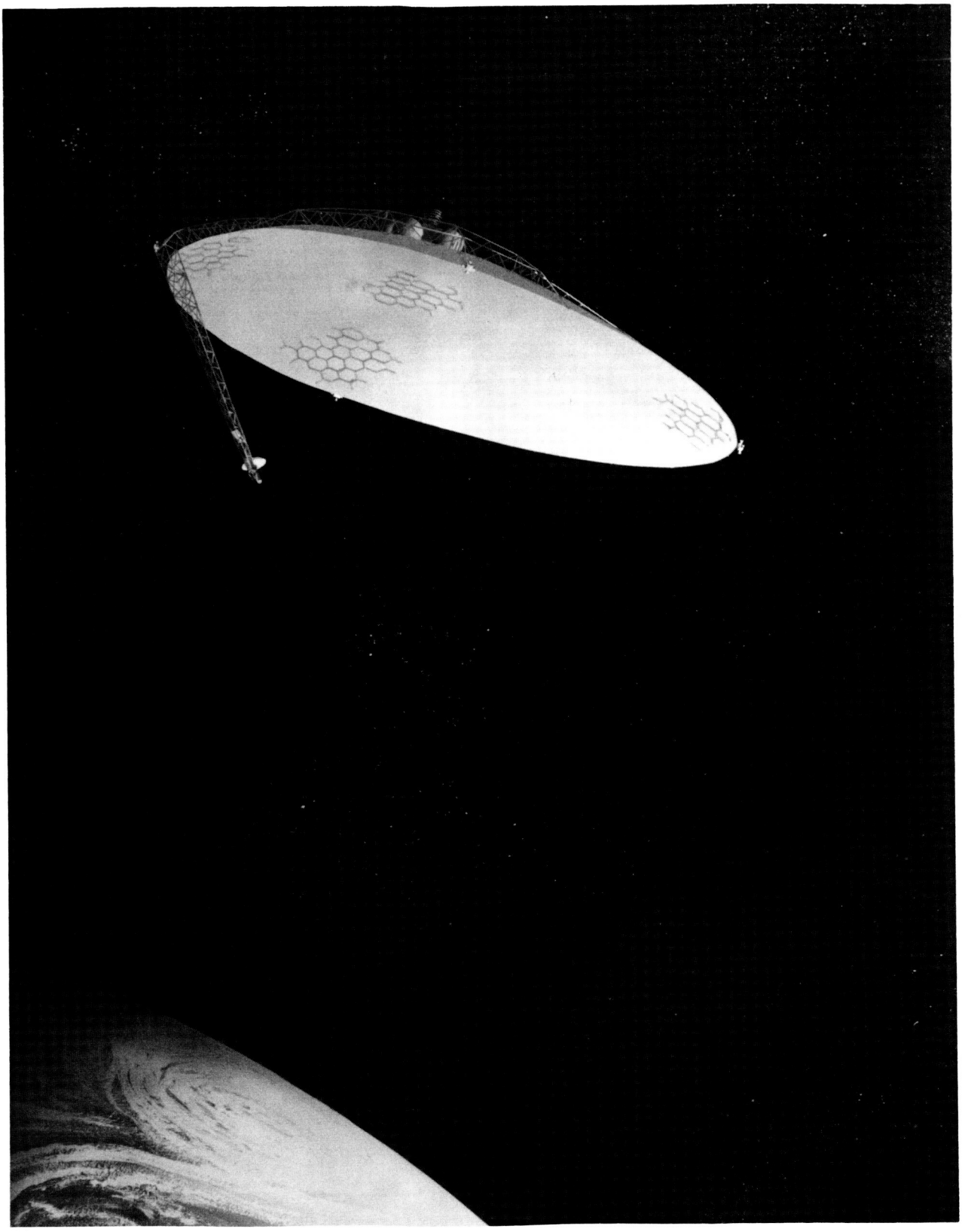

Figure 7. Conceptual Figure of a Geostationary Antenna

For geostationary observations, the offset, prime-focus antenna configuration has no peer: it features wideband operation (octave bandwidths) with minimum physical blockage and spillover. The collecting aperture is characterized as a real, filled aperture. To the extent that spillover does occur, the radiation is directed principally toward the cold Cosmic Background rather than toward the warm radiating surfaces on the planet. Antenna steering is accomplished by gyros and stabilized reaction wheels which are augmented by gas jets, as shown in the figure.

The search pattern that is shown in Figure 5 required a movement of the collecting aperture of only 0.93 degrees in two axes to execute a search pattern containing 1140^2 kilometers^2 at 55 degrees latitude. The thrust from the booster assembly that is shown on the back of the aperture is used to enable initial positioning in orbit and to execute orbital maneuvers.

When there is an advantage to do so, and when degraded antenna performance is tolerable, the antenna configuration may be converted into an offset Cassegrain by affixing a secondary mirror at the prime focus. When the secondary mirror is illuminated non-symmetrically, rotation of the mirror produces a narrow spiral beam movement which may be applied for localized search operations, id est, to image the area contained within an isthmus or harbor.

The conceptual design of an antenna system that is supported by a two-axis mount is shown in Figure 8. The mount supports an offset, prime-focus antenna configuration whose collecting aperture is here assigned the perspective dimension of 1.5 meters to elucidate the conceptual representation of the overall proportions of the physical structure. In practice, the diameter of the collecting aperture and the antenna components are scalable to the extent that they are bounded by practicality. The two-axis mount and the collecting aperture are readily scalable to large apertures that are consistent with the detection models that are discussed in this monograph (30.48 meters). The two-axis mount is immediately recognizable as a conventional elevation-over-azimuth type that is eminently capable of arc-second pointing capability. As it is shown, the mount is supported on the underside of a geostationary spacecraft.

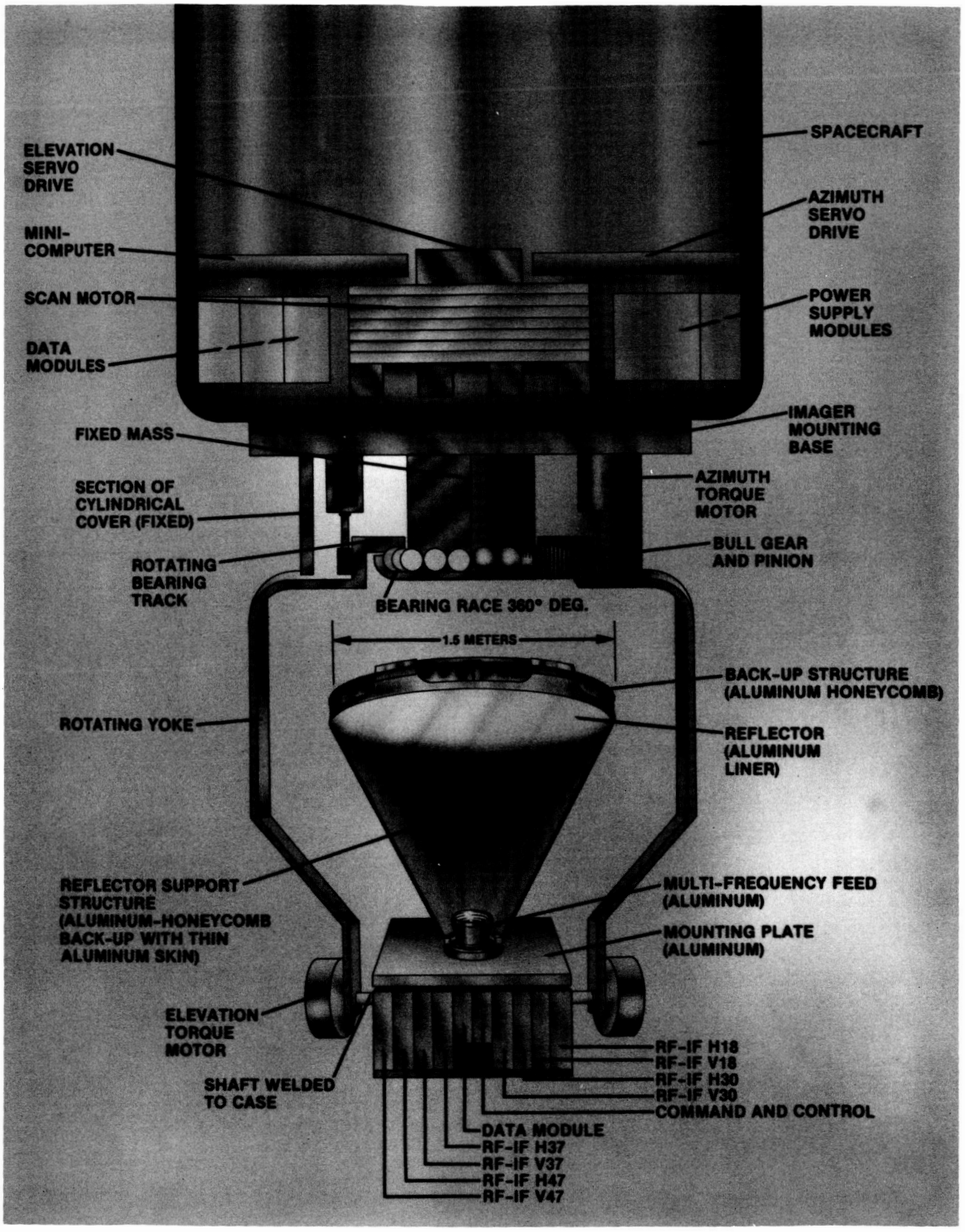

Figure 8. Conceptual Figure of a Two-Axis Mount With an Offset, Prime-Focus Antenna That Is Attached to a Geostationary Spacecraft

Many other antenna configurations are adaptable to the requirements and needs of geostationary antennas. The examples given here are driven by the need for stiff, stable, cantilevered structures that feature real, filled collecting apertures that are capable of wideband operation at microwave wavelengths.

The detection of particular and isolatable objects that exist on planetary surfaces, on the surfaces of their natural satellites, and from within their sensible atmospheres is the principal concern of this monograph. Categories of emitting and metal objects are identified, complete with the mathematical expressions that explain the statistical precision (S/C) of their individual measurements. The S/C ratio (an arbitrarily derived quantity) that is concomitant with the measurement of any object or phenomenon is of critical importance: from the S/C, the precision and accuracy of the intrinsic (innate) properties of the object are estimated.

Detection of objects on the planetary surface from geostationary altitude is achieved by application of the Microwave Power Transfer Equations (derived here), which are known by the cognoscenti to be a particular mathematical form that is similar to the familiar Radar Range Equations.

The morphology and application of the Microwave Power Transfer Equations that are derived here--and including some that are excerpted from the references--show, in summary:

Detection criteria are determined as follows:

- Source of the available microwave power is identified. Microwave power is construed also as heat, flux, or energy.

- Magnitude of the available microwave power is determined.

- Direction of propagation of the microwave power flow is explained by the Laws of Thermodynamics.

- Field interception and field reradiation from metal objects are shown to possess bistatic scattering properties.

- Ultimate destination of the microwave power that is reradiated from metal objects is identified.

Separate thermodynamic temperature transfer equations are given for:

- Metal objects
  Aircraft, spacecraft, ships, buoys
  Cities, antenna sites, astrodomes

- Cold emitting objects
  Wake, currents, eddies, rivers, lakes

- Warm emitting objects
  Wakes, currents, eddies, deserts, forests

The equivalence between microwave power and thermodynamic temperature is expressed by:

- The Planckian approximation to the Planck Radiation Function [2,7]:

  $$P = k\,T, \text{ in watts/hertz}$$

  where

  k = Boltzmann Constant, in joules

  T = Thermodynamic temperature, in kelvins

The rate of increase in the power density in the radiated field of an emitting blackbody (also a graybody) is expressed by:

o The Stephan-Boltzmann equation [6]:

$$W = [\varepsilon]\ [\sigma]\ T^4, \text{ in watts/hertz}$$

where

ε = Emissivity

σ = Stephan-Boltzmann constant

T = Thermometric temperature of the emitting surface, in kelvins

The direction of microwave power flow is controlled and explained by:

o Zeroth Law of Thermodynamics

o Second Law of Thermodynamics

The thermodynamic properties of surface materials are explained by:

o The fundamental complementary thermodynamic equality:

$$1 = \alpha + \varepsilon + \rho$$

where

α = Absorptivity

ε = Emissivity

ρ = Reflectivity (sometimes called transmissivity)

Detection applications are as follows:

- Planet-orbiting vehicles
- Geostationary platforms

FOOTNOTES

[1] The Laws of Thermodynamics are four:

The Zeroth Law states, in the main, that if two bodies are in thermal equilibrium with a third, then all bodies are in thermal equilibrium with each other.

The First Law deals with the basic relationships existing among heat, work, and entropy. The First Law has no direct relevance to the material contained within this monograph.

The Second Law states, in the main, that a warm body radiates heat to a cooler body and it is never the other way around. The law is driven by the principle that heat seeks cold and that it is never the other way around. Once the heat transfer process commences, the direction is irreversible. A generalization of experimental fact shows that natural processes occur spontaneously in one direction only and that they are irreversible.

The Third Law of Thermodynamics states, in the main, that it is impossible, by any procedure--no matter how idealized--to reach absolute zero in any finite number of operations. The Third Law has no particular relevance or application in this monograph; it is included for completeness and for illustration of the fact that some of the important laws of physics are based on experience and observation. The Cosmic Background (2.7 kelvins) is the coldest natural phenomenon that is available for use or observation by a microwave system.

The Laws of Thermodynamics are credited to no man: they are conceived and tested by experience and practice. If an exception is found to a law, it will cease to exist.

The Laws of Thermodynamics are critically important in the practice and application of microwave systems: mainly, the laws define the conditions that are required to produce thermal equilibrium among physical bodies and they show the direction of heat (flux and power) flow through microwave systems and power transmission components.

The numerical order of the Laws of Thermodynamics varies somewhat in the technical literature, and there are a few laws that are not summarized here.

2 The term "thermodynamic sensors" is defined as a class of sensors that respond to the fluxes produced by the radiances and irradiances of natural sources. The transport of energy among natural sources is controlled by the Zeroth and Second Law of Thermodynamics. A microwave receiver is categorized as a thermodynamic sensor.

The volume contained (mainly) within the principal lobe of an antenna pattern (scene) operates as a source of microwave power, au fond, graybody radiation. The integrated value of the radiant emittances (microwave flux, or power, per unit area) that are contained within the volume of the scene may be equivalently construed as a thermodynamic temperature which is dimensioned in units of kelvins. Microwave flux and thermodynamic temperature are equivalent (transformable) quantities: they are related quantitatively in the terms of the Planckian Function [2].

Through the reciprocal properties of the antenna-gain function, the integrated thermodynamic temperature of the scene is in thermal equilibrium with the impedance at the phase center of the antenna, a condition that is controlled by the Zeroth Law of Thermodynamics.

Thermodynamic sensors respond to emitting objects and metal objects that intrude into the volume of the scene. When an emitting object, exempli gratia, a warm eddy on the sea surface, intrudes into the scene, the radiant emittance produced by the warm eddy transfers heat (thermodynamic temperature) to the impedance at the phase center of the antenna and disturbs

the state of equilibrium existing between the scene and the phase center of the antenna. The warm eddy transfers its heat to the phase center of the antenna as it is controlled by the Second Law of Thermodynamics, id est, a warm body (eddy) radiates heat and the cold body (impedance at the phase center) absorbs it, and the process is irreversible.

A thermodynamic sensor responds to the intrusion of a metal object into the scene: microwave power (flux) is transferred from the impedance at the phase center of the antenna to the Cosmic Background through the bistatic-gain properties of the metal object. The direction of the microwave power transfer (heat) is controlled by the Second Law of Thermodynamics. The magnitude of the total gain that is involved in this power transfer need be appreciated: it typically exceeds 100 dB.

Consider that the gain of a 30-meter-diameter antenna exhibits 80 dB of gain at an operating wavelength of 8 millimeters and that the incident and forward (bistatic) gains of a large aircraft may each possess more than 60 dB--all operate to affect the heat transfer from the phase center of the antenna to the Cosmic Background.

The input terminals of the thermodynamic sensor are connected electrically to the impedance at the phase center of the antenna. Variations in the thermodynamic temperature transfer relationships existing across the impedance at the phase center are linearly manifested in the output terminals of the thermodynamic sensor (microwave receiver).

The microwave power levels that originate from the radiances and irradiances of natural sources are particularly interesting and informative. Consider that the mean thermodynamic temperature of a scene is 290 kelvins and that a mechanism is provided to transfer this heat to the Cosmic Background, which is known to be a blackbody at 2.7 kelvins--in the microwave region. From the Planckian Function approximation, which applies to the microwave region, the microwave power available for transfer is given by

$$P = k\,T, \text{ in watts/hertz}$$

where

$k = 1.38046 \times 10^{-23}$ joules, the Boltzmann Constant

T = Thermodynamic temperature of a blackbody, in kelvins

Given that the thermodynamic temperature of the scene is 290 kelvins and that the Cosmic Background is 2.7 kelvins, then the microwave power available for transfer in a 100-megahertz noise bandwidth, B_n, is

$$P = k\,T\,B_n, \text{ in watts}$$

$$= k\,(290 - 2.7)\,(100 \times 10^6), \text{ in watts}$$

$$= 397 \text{ femtowatts}$$

Given that the thermodynamic temperature resolution of a microwave receiver is 1 kelvin (1-σ noise), then the power level of the noise, P_n, as it is referred to the input terminals, within the same 100-megahertz noise bandwidth, is

$$P_n = k\,(1)\,(100 \times 10^6), \text{ in watts}$$

$$= 1.38 \text{ femtowatts}$$

Apparently, from this example, the ratio of available microwave power that is produced by the irradiances of natural sources, P, to the noise power of the receiver, P_n, is expressed by

$$\frac{P}{P_n} = \frac{(397)}{(1.38)} = 288\ (25\ \text{dB})$$

The microwave system equations that utilize natural power sources for detection are developed in [3].

3

The term "scene" is defined as the volume contained within the 3-dB-gain pattern of the principal lobe of the antenna. The scene contains the radiant emittances (fluxes/unit area) from the surface and its features and from the gaseous emissions and the water particulates in the atmosphere. In the argot of the infrared artform, the pixel is similar in concept to the scene.

The thermodynamic temperature of the scene is in thermal equilibrium with the impedance at the phase center of the antenna. The condition of thermal equilibrium, existing between the scene and the impedance at the phase center of the antenna, is in conformance with, and is controlled by, the Zeroth Law of Thermodynamics [4]. The equivalence between radiant emittance (which is also construed as flux or microwave power per unit area) and thermodynamic temperature is expressed, in closed form, by the Planckian function [2].

The total radiant emittance of the scene is the source of energy (equivalently, a thermodynamic temperature) that furnishes microwave power for the detection of metal objects and cold surface features. Microwave power is transferred from the impedance at the phase center of the antenna to the Cosmic Background through the bistatic-gain properties of a metal object. The direction of the power transfer is controlled by the Second Law of Thermodynamics [4].

The terms scene and instantaneous field of view (IFOV) are used interchangeably in this monograph depending upon the context of the material under discussion. A "swath" is defined as a line of conterminous scenes. In the perspective of a matrix, a swath is regarded as a row rather than as a column. The "field of view" (FOV) is the angular subtense of a swath as it is viewed by the phase center of an antenna. The phase center of the antenna operates electrically as a point source of radiation.

REFERENCES

[1] C. W. Allen, Astrophysical Quantities, Second Edition, University of London, The Athalone Press, 1963.

[2] J. M. Stacey, Microwave Blackbodies for Spaceborne Receivers, JPL Publication 85-10, March 1, 1985.

[3] J. M. Stacey, Target Detection Using the Irradiances of Natural Sources, JPL Publication 84-70, November 15, 1984.

[4] J. M. Stacey, Spaceborne Microwave Imagers: Principles and Practices, JPL Publication 86-37, November 1, 1986.

[5] J. M. Stacey, Microwave Properties of a Quiet Sea, JPL Publication 85-33, May 15, 1985.

[6] J. M. Stacey, Power Transfer From Natural Emitters to Collecting Apertures at Microwave Wavelengths, JPL Publication 84-48, December 1984.

[7] J. M. Stacey, Spaceborne Microwave Receivers: Principles and Practices, JPL Publication 84-49, October 1, 1984.

APPENDIX A

SHORT-PULSE-RADAR OBSERVATION OF AN AIRCRAFT

This appendix deals with the modeled detection of an aircraft by a short-pulse radar from geostationary altitude. The radar operates in the functional mode of a microwave imager as illustrated and discussed in Figure 5.

It is well-known within the radar community that the S/N ratio degrades in proportion to the fourth power of the slant range. For this reason alone radars that operate in geostationary orbit are severely disadvantaged, because all slant ranges exceed 35,760 kilometers (see Figure 3).

It is imprudent at this time to conclude categorically that radar sensors fail a detection from geostationary altitude because of slant ranges alone. It is better to examine all of the terms in the system-performance equations to determine where radar detection capability is lacking, limited, or marginal, and by how much. From this approach, informed estimates can be applied more efficaciously to size the radar equipment from the standpoint of feasibility, practicability, and state of the art.

The system performance is described here for a very basic, simple short-pulse radar. From this rudimentary model, radar capability is more easily estimated and its parameters are readily scalable to radar configurations possessing greater sophistication.

Synthetic-type and side-looking radars are categorically excluded from consideration as geostationary sensors; mainly, they fail because critical and essential signal properties such as range-rate or doppler-differences do not exist in the data.

The operating wavelength for all sensor systems considered in the models of this monograph is 8 millimeters. Similarly, the area of the collecting aperture (A_c) is arbitrarily specified at 730 meters^2, which is, equivalently, the area of a 30-meter-diameter paraboloid. The antenna efficiency, ϵ, of the collecting aperture is specified at 0.55. From this, the antenna gain, G, is computed to be 78.9 dB.

The collecting aperture of the antenna is characterized as a real, filled aperture which is physically blocked by a secondary reflector and pods. By expectation, spillover losses occur around the perimeter of the collecting aperture. The antenna efficiency is perceived as an operator that modifies the area of the collecting aperture. The antenna efficiency specifies the percentage of the collecting area that is available to produce on-axis gain.

Figure A-1 illustrates a useful and interesting chart that organizes microwave antenna systems by hierarchies. The chart is excerpted from [4] and reproduced here. From the chart, the short-pulse radar is described by a 0000 characteristic code.

A symmetrical Cassegrain antenna configuration is chosen for the radar model because of its pandemic acceptance and widescale application in the radar community.

A functional schematic diagram of the short-pulse radar is shown in Figure A-2. The diagram identifies the dissipative losses that are associated with the radar components. The loss symbols are also defined.

The radar transmitter operates at a peak power level, P, of 1 kilowatt and with a pulse width (τ) of 1 microsecond. The peak-power specification is reasoned to be consistent with a solid-state transmitter which is peak-power limited. The radar configuration is perceived as a simple, basic type whose performance can be readily and easily scaled to more sophisticated radar configurations by investigators who opt to draw comparisons.

The observed aircraft--used in the short-pulse radar model--is characterized as a CV-990/B-707 type, which is perceived to operate within the imaged area shown in Figure 5 at 55 degrees latitude and at slant range of 38,288 kilometers. The total projected area of the top surfaces of the wing, fuselage, and tail sections of the aircraft, as viewed from the coign of vantage of a geostationary-borne radar, is 382 meters^2. The total projected

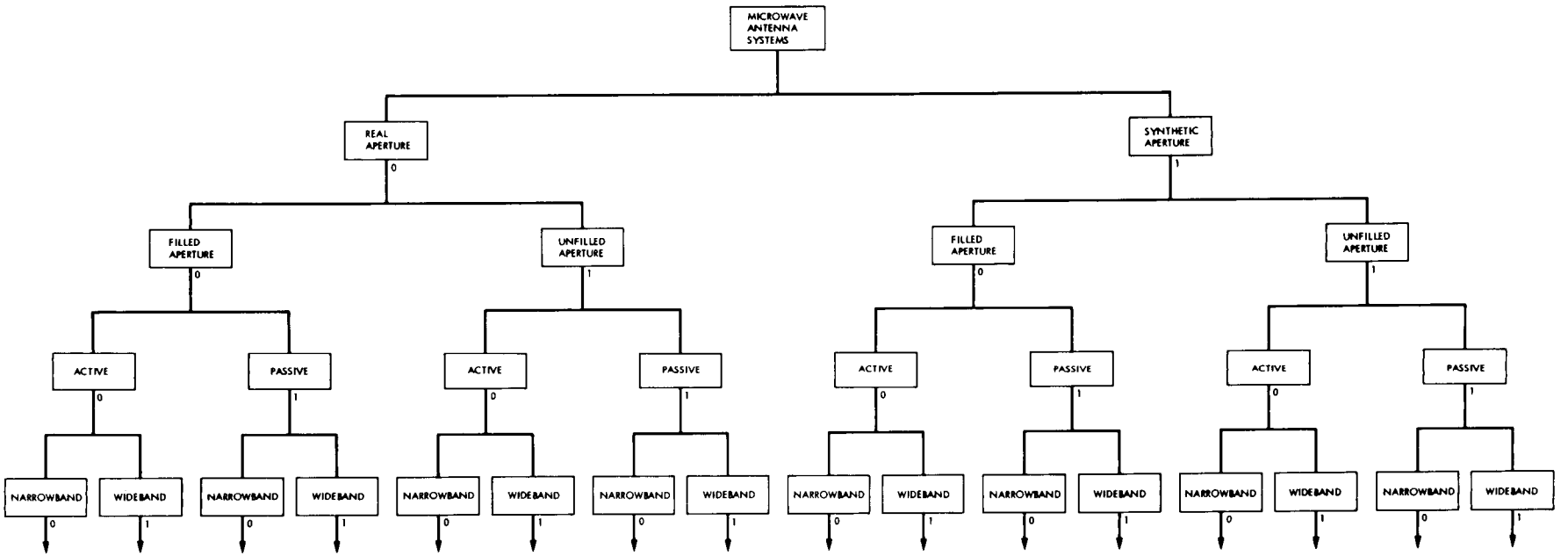

Figure A-1. Hierarchy of Microwave Imaging Systems. The hierarchy of microwave imaging systems is taken from Reference [7], Figure 240, where its structure is discussed and critical terms are defined. The figure is reproduced here as a convenience, to show where in the hierarchy of microwave imagers the geostationary sensors lie.

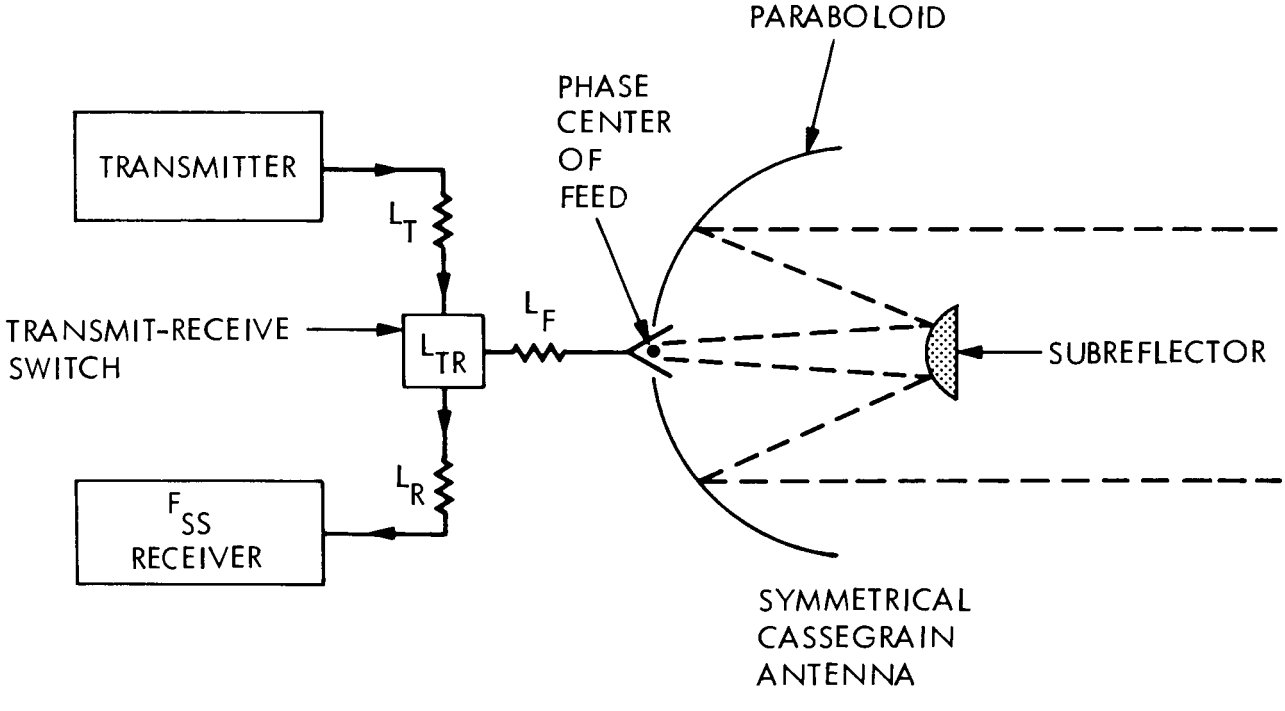

Figure A-2. Functional Schematic Diagram of a Short-Pulse-Radar Sensor

area of the top surfaces (normal incidence) of the aircraft is defined as the monostatic, backscattering cross-section (σ).

The most critical parameter affecting detectability of the aircraft is the expected value of the signal-to-noise ratio (S/N). From the S/N--assuming that it is large and positive--the precision and accuracy of the radar measurement is determined, along with the probability of detection.

The classical procedure to be applied at this juncture is to compute the range equations for the radar performance and also the system operating temperature, T_{sys}, from the receiver losses. T_{sys} is calculated by first using the symbolized losses given for the radar as shown in Figure A-2 and by following the procedures outlined in Reference [7], Figure 5.

The atmospheric loss terms that are included in the expression of T_{sys} are taken from the thermodynamic model and from the example given in [4]. The atmospheric model and the example are reproduced as Figures A-3 and A-4, respectively.

The course of the analysis for the performance of the short-pulse radar is to first compute the system temperature of the receiver, T_{sys}, and then determine the receiver-noise power, P_n, where it is referenced to the input terminals of the receiver. Subsequently, the signal power that is contained within the echo from the CV-990/B-707 aircraft, P_{sig}, is computed. The ratio expressed by P_{sig}/P_n is defined as the signal-to-noise (S/N) ratio for the measurement.

Insofar as it is practicable, the equations are maintained in expanded form to show the relative loss contributions for each term when taken separately for the radar equipment, as illustrated in Figure A-4. From the atmospheric loss models given in Figures A-3 and A-4, and from the radar equipment model given in Figure A-2, we adopt the thermodynamic temperature of the atmosphere and the sea surface at 129 kelvins, T_{sea}, as the thermodynamic temperature of the background for a clear day and at 8-millimeters wavelength.

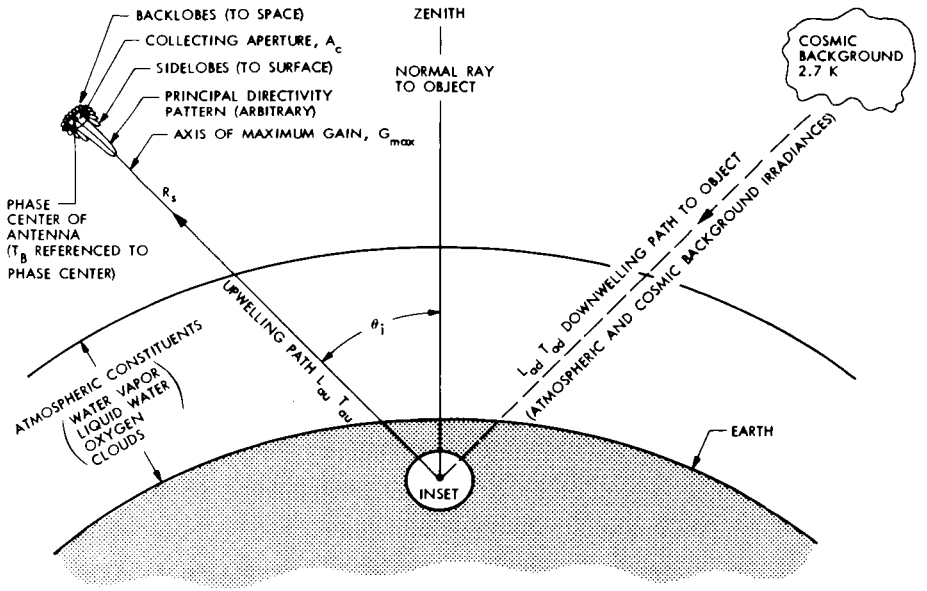

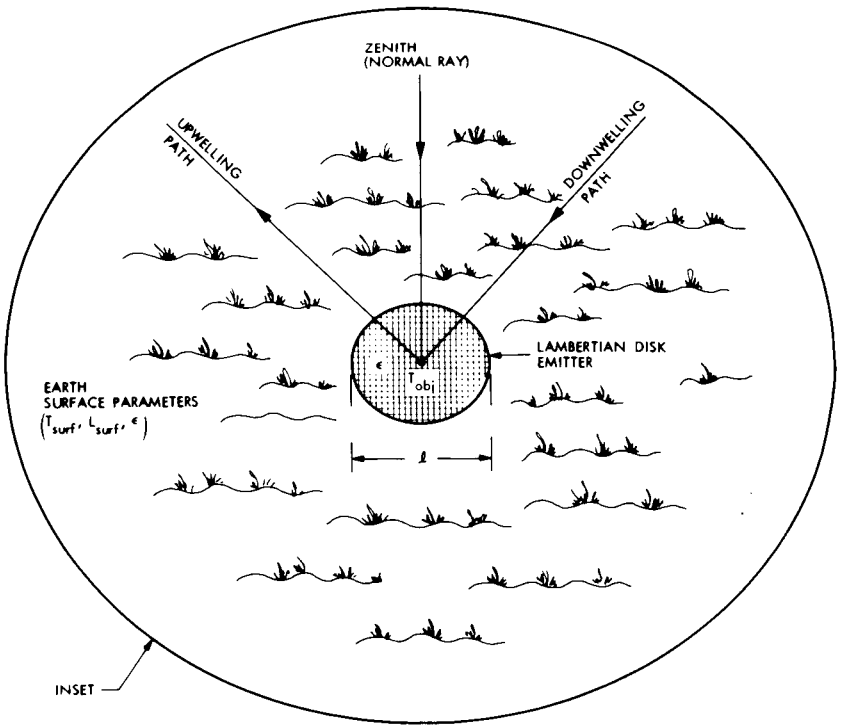

LEGEND

T_{au} = INTEGRATED PHYSICAL TEMPERATURE OF THE UPWELLING PATH, K

L_{au} = LOSS IN THE UPWELLING PATH

T_{surf} = PHYSICAL TEMPERATURE OF THE SURFACE MATERIAL, K

L_{surf} = LOSS IN THE SURFACE MATERIAL

T_{ad} = INTEGRATED PHYSICAL TEMPERATURE OF THE DOWNWELLING PATH, K

L_{ad} = LOSS DOWNWELLING PATH, K

T_B = THERMODYNAMIC TEMPERATURE OF THE BACKGROUND, K

T_{obj} = TEMPERATURE OF OBJECT (UNIFORM), K

ϵ = EMISSIVITY OF OBJECT

α = ABSORPTIVITY OF OBJECT

ℓ = DIAMETER OF OBJECT, m

R_s = SLANT RANGE (COLLECTING APERTURE TO OBJECT), m

A_c = AREA OF COLLECTING APERTURE, m^2

G_{max} = AXIS OF MAXIMUM ANTENNA GAIN

θ_i = INCIDENCE ANGLE, deg

$$T_B = \underbrace{\frac{T_{cosmic}}{L_{ad}\,L_{surf}\,L_{au}}}_{[\text{COSMIC}]} + \underbrace{\frac{T_{ad}\,(L_{ad}-1)}{L_{ad}\,L_{surf}\,L_{au}}}_{[\text{DOWNWELLING}]} + \underbrace{\frac{T_{surf}\,(L_{surf}-1)}{L_{surf}\,L_{au}}}_{[\text{SURFACE}]} + \underbrace{\frac{T_{au}\,(L_{au}-1)}{L_{au}}}_{[\text{UPWELLING}]}, \text{K}$$

WHERE: ϵ = EMISSIVITY

$$L_{surf} = \frac{1}{1-(\epsilon+\alpha)}$$

SUBCRIPTED L SYMBOLS ARE DISSIPATIVE LOSSES EXPRESSED AS A NUMBER > 1.

Figure A-3. Thermodynamic Model of Atmospheric Loss Media

$$T_B = \underbrace{\frac{T_{COSMIC}}{L_{ad}\,L_{surf}\,L_{au}}}_{[\text{COSMIC}]} + \underbrace{\frac{T_{ad}\,(L_{ad}-1)}{L_{ad}\,L_{surf}\,L_{au}}}_{[\text{DOWNWELLING}]} + \underbrace{\frac{T_{surf}\,(L_{surf}-1)}{L_{surf}\,L_{au}}}_{[\text{SURFACE}]} + \underbrace{\frac{T_{au}\,(L_{au}-1)}{L_{au}}}_{[\text{UPWELLING}]}\text{, KELVINS}$$

$$= \frac{2.7}{(1.08)(1.54)(1.08)} + \frac{280\,(1.08-1)}{(1.08)(1.54)(1.08)} + \frac{290\,(1.54-1)}{(1.54)(1.08)} + \frac{280\,(1.08-1)}{(1.08)}\text{, KELVINS}$$

$$= (1.5) + (12.47) + (94.16) + (20.74)\text{, KELVINS}$$

$$= 128.87 \text{ KELVINS}$$

ASSUMPTIONS FOR A CLEAR QUIET SEA AT MID LATITUDE.

$T_{COSMIC} = 2.7$ K

$L_{ad} = L_{au} = 0.35$ dB (1.08)

$(\epsilon + \alpha) = 0.35$ (ARBITRARY POLARIZATION)

$L_{surf} = \frac{1}{1-(\epsilon+\alpha)} = 1.54$

$T_{ad} = T_{au} = 280$ K

$T_{surf} = 290$ K

Figure A-4. Thermodynamic Temperature Transfer Model for a Clear Day at 8-millimeters Wavelength

The atmospheric and sea-surface loss models, as illustrated in Figures A-3 and A-4, are calculated for an angle of incidence, θ_i, of 50 arc-degrees. The angle of incidence at 55 degrees latitude from geostationary altitude is 57 degrees (see Table 1--this is an insignificant difference for modeling purposes).

The expression for T_{sys} is written

$$T_{sys} = T_{sea} + T_A(L_A - 1) + L_A T_f(L_f - 1) + L_A L_f T_{TR}(L_{TR} - 1) + L_A L_f L_{TR} T_R (L_R - 1) + L_A L_f L_{TR} L_R T_m (F_{ss} - 1), \quad \text{in kelvins} \tag{A-1}$$

where

T_{sea} = Thermodynamic background temperature of the sea and the atmosphere, given as 129 kelvins from Figures A-3 and A-4.

T_A = Thermometric temperature of the collecting surfaces of a symmetrical Cassegrain antenna to which the gain losses are referenced. The 290-kelvin temperature is adopted to be consistent with the international-standard thermometric temperature for noise figure measurements, id est, 290 kelvins.

L_A = Collecting aperture losses that are caused by blockage and spillover for a symmetrical Cassegrain antenna. When the antenna efficiency factor, ϵ, is specified at 0.55, the antenna gain is reduced by 45%--equivalently, a loss factor of 1.61 dB.

T_f = Thermometric temperature of the feed and the waveguide connections, 290 kelvins.

L_f = Dissipative losses in the feed structure and the associated waveguide connections, 1.0 dB.

T_{TR} = Thermometric temperature of the dissipative losses in the transmit-receive switch, 290 kelvins.

L_{TR} = Dissipative loss of the transmit-receive switch, 1.0 dB.

T_R = Thermometric temperature of the waveguide loss between the transmit-receive switch and the mixer unit in the receiver, 290 kelvins.

L_R = Dissipative loss in the waveguide between the transmit-receive switch and the mixer unit in the receiver, 1.0 dB.

T_m = Thermometric temperature of the mixer, 290 kelvins, the standard thermometric temperature to which all noise figure measurements are referenced.

F_{ss} = Single-sided noise figure [7] of the mixer unit, 7.0 dB.

From Equation (A-1), when

$$T_A = T_f = T_{TR} = T_R = T_m = 290$$

and (A-1) simplifies to

$$T_{sys} = [290]\ [L_A L_f L_{TR} L_R F_{ss} - 1], \quad \text{in kelvins} \qquad \text{(A-2)}$$

by substitution of the numerical quantities defined above in (A-2),

$$T_{sys} = (129) + (290)\left(10^{\frac{1.61}{10}}\ 10^{\frac{1}{10}}\ 10^{\frac{1}{10}}\ 10^{\frac{1}{10}}\ 10^{\frac{7.0}{10}} - 1\right), \quad \text{in kelvins}$$

which reduces to

$$T_{sys} = 129 + 3911 = 4040, \quad \text{in kelvins}$$

The predetection noise-bandwidth, β_{opt}, of the receiver, and the transmitter pulse-width, τ, are related by

$$\tau \beta_{opt} = 1.2 \qquad \text{(A-3)}$$

where

τ = Pulse width, in seconds

β_{opt} = Predetection bandwidth, in hertz

For the case when the receiver is operating near threshold sensitivities [A-1], given that

$$\beta_{opt} = \frac{1.2}{\tau},$$

the optimum noise-bandwidth for the radar receiver, and where τ is a 1-microsecond transmitted pulse-width,

β_{opt} = 1.2 megahertz

The noise power level, P_n, for the receiver, where it is referenced to the input terminals, is expressed by

$$P_n = k T_{sys} \beta_{opt}, \text{ in watts} \qquad \text{(A-4)}$$

where $k = 1.380662 \times 10^{-23}$ joules/kelvin, the Boltzmann Constant, and where P_n is defined as the receiver noise power in the predetection bandwidth.

By substituting numerical values in (A-4)

$P_n = 66.9 \times 10^{-15}$, or 66.9 femtowatts

The signal power, P_R, that is returned within the echo from the aircraft is expressed by

$$P_R = P\ G\ \frac{1}{4\pi\ R_s^2}\ [(\sigma\ Z_r)(\cos\ \theta_i)]\ \frac{1}{4\pi\ R_s^2}\ A_c\ \frac{1}{L_T\ L_{TR}\ L_f},\ \text{in watts} \qquad \text{(A-5)}$$

noting that L_t, L_{TR}, and L_f are the dissipative losses for the transmitter path. Notably, the dissipative losses for the receiver path are embedded in the system temperature, T_{sys}.

By collecting and recasting terms and by introducing the radar-transmitter equipment losses, we obtain

$$P_R = \frac{P\ G\ [(\sigma\ Z_r)(\cos\ \theta_i)]\ A_c}{(4\pi\ R_s^2)^2\ L_T\ L_{TR}\ L_f},\ \text{in watts} \qquad \text{(A-6)}$$

given that

P = 1 kilowatt, the transmitter power, in watts.

G = The transmitting antenna gain, 78.9 dB, based on an area of 730 meters^2 for the collecting aperture and with an antenna efficiency factor, ε, of 0.55 at an operating wavelength of 8 millimeters. Antenna gain is expressed as a dimensionless quantity.

ε = 0.55, the antenna efficiency factor, which expresses the fraction of the collecting area that is available to produce gain. The available collecting area is diminished by the effects of physical blockage from pods, secondary reflectors, and dissipative losses within the antenna structure itself. The antenna efficiency factor also includes the effects of spillover around the edge of the collecting aperture and participating secondaries.

σ = 382 meters^2, the projected area of the topside view of the CV-990/B-707 aircraft.

Z_r = 0.06, the reflectivity factor, which expresses the fraction of the area of the target that participates in intercepting and rescattering the incident flux from the radar transmitter. The numerical factor 0.06 is consistent with the empirically derived monostatic backscatter coefficient returned by many aircraft structures. In the vernacular of the radar art, the reflectivity factor is given as -12.2 dB below 1 meter^2 for certain conventional aircraft. The reflectivity factor is determined empirically, and the term denotes that it is a statistical term that contains intrinsic, non-stationary moments. The reflectivity factor is applied in the power transfer equations as an operator to reduce the total area of the aircraft at the aspect it is viewed at by the radar.

θ_i = 57 degrees. The angle of incidence operates on the projected area of the aircraft to reduce its area, depending upon the aspect that it is viewed at by the radar. At 55-degrees latitude, the aircraft is viewed by the radar at an incidence angle of 57 degrees.

A_c = 730 meters^2, the collecting area of the Cassegrain paraboloid.

R_s = 38,288 kilometers, the slant range to 55-degrees latitude.

By substitution in (A-6),

$P_R = 1.045 \times 10^{-18}$ watts, or 1.05 attowatts

The S/N ratio produced by the CV-990/B-707 aircraft at 55-degrees latitude is expressed by

$$S/N = P_R/P_n = 1.895 \times 10^{-18}/66.9 \times 10^{-15}$$

$$= -48.06 \text{ dB}$$

--notably, a large, negative, and dimensionless quantity.

The modeled analysis and the calculations that are produced in this appendix serve as the primitive source material for the short-pulse radar that is discussed and epitomized in Section 5.1.

APPENDIX A

REFERENCES

[A-1] E. M. Purcell, Chapter 2, "The Radar Equation," in L. N. Ridenour, ed., Radar System Engineering, MIT Radiation Laboratory Series, McGraw-Hill Book Company, New York and London, 1947.

APPENDIX B

THERMODYNAMIC OBSERVATION OF METAL OBJECTS ON A SEA BACKGROUND

The detection of a large aircraft that is operating over a sea background from geostationary altitude is the subject of this appendix. Considered here are the critical factors that affect the modeled detection of a CV-990/B-707 aircraft that is operating above the atmosphere of the planet.

The methodology of the analysis employs the transport of microwave power which is derived from the irradiances and radiant emittances of natural sources. Microwave power is available from the thermodynamic difference in temperatures existing between natural sources. The transport of power within the microwave transmission system is controlled and influenced by the Zeroth and Second Laws of Thermodynamics.

Microwave power, flux, and thermodynamic heat are similarly construed: they are related by the Boltzmann Constant and modified by variations in the predetection noise bandwidth. Changes in these quantities occur in synchronism and instantaneously.

Microwave power (flux) is construed as a source of heat. The direction of the heat flow is controlled by the Laws of Thermodynamics. Once the heat transfer starts, the direction of propagation is known to be irreversible and the heat flow continues until a state of thermal equilibrium is reached.

Metal objects are endowed with bistatic microwave scattering properties. When the myriad collecting areas of an arbitrary irregular metal object intercept an arriving wavefront, a pattern of creeping currents suffuses the entire surface of the metal object. The creeping currents excite the multiple metal facets of the object, and a reradiation pattern results that is uncorrelated with the incident wavefront. A pattern of radiating point sources is set up in the surfaces of the metal object whose electrical characteristics and directivities are explained by the Kirchhoff-Huygens Principle of reradiation from distributed sources [4]. The direction from which

the incident wavefront arrives and the direction of the reradiated wavefront (forward scatter) are controlled by the Second Law of Thermodynamics. The microwave power contained in the incident waveform and in the reradiated wavefront is reckoned in units of watts/meter^2.

It is critically important to comprehend and to appreciate that the power density of an incident microwave waveforms is not reflected from a metal object; rather, the reradiation pattern is produced by the electrical properties (Kirchhoff-Huygens Principle) of the metal surfaces. The detailed structure of the lobes of the reradiated pattern (directivities) depends upon the physical orientation (disposition, albeit random) of the facets of the metal surfaces and the magnitudes of the current wavelets that suffuse the metal surfaces. Current wavelets are construed as point sources whose fields diffract and interfere to produce reradiated lobes.

The forward-scattered reradiation patterns from aircraft and ships are illustrated conceptually in Figure B-1.

With consideration of these prefatory remarks concerning the character of the expected response (signature) of a metal object, let us proceed to calculate the S/N ratio of a CV-990/B-707 type of aircraft that operates in level flight at an altitude that is unaffected by the attenuating layers of the atmosphere.

The modeled observation of the aircraft signature is powered by the available flux that is produced by the irradiances and radiant emittances of natural sources. The thermometric sensor operates from geostationary orbit while it executes a continual search pattern as shown in Figure 5.

The level of the available power is given by:

$$P_{av} = k(T_{pc} - T_{Cos})\, B_n, \quad \text{in watts} \qquad \text{(B-1)}$$

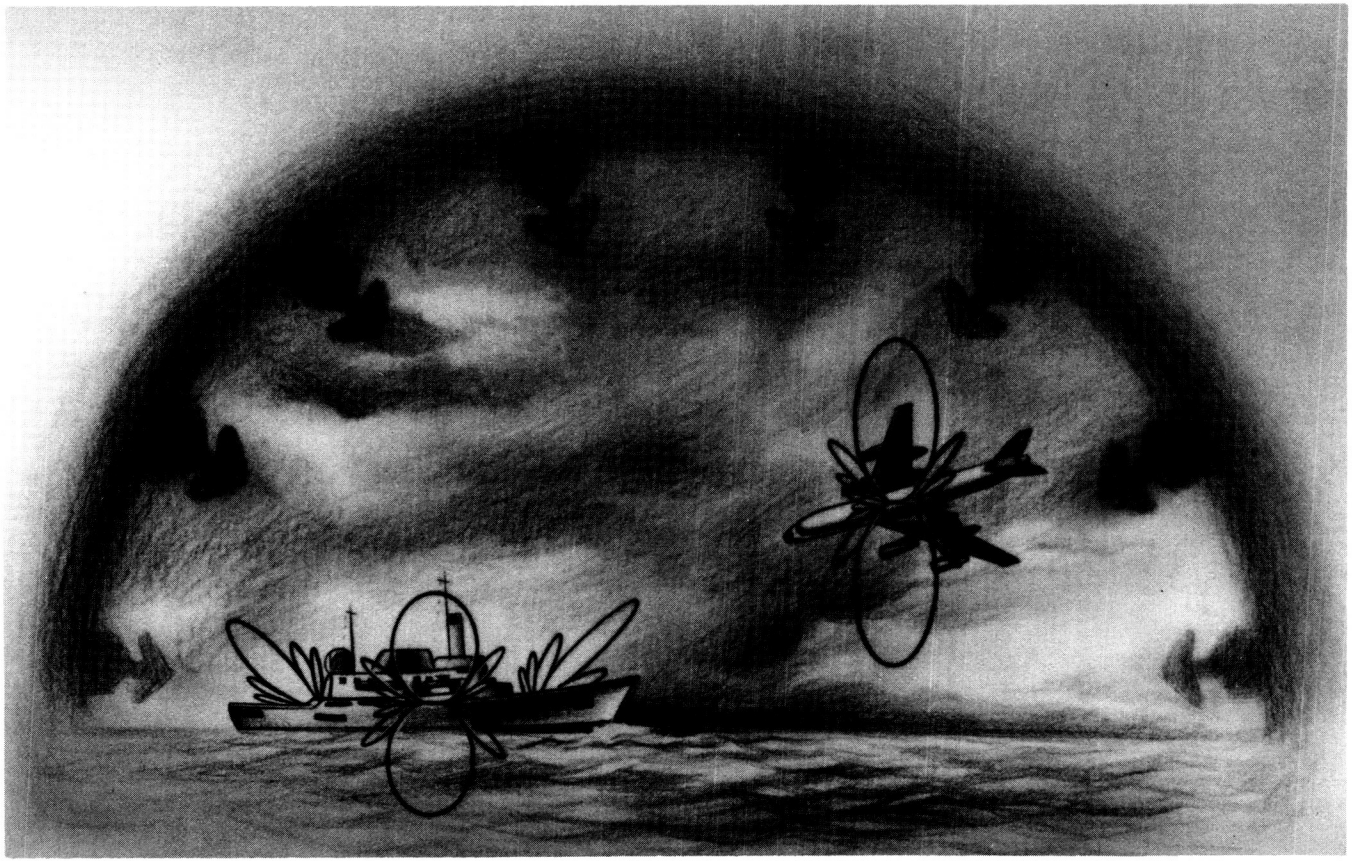

Figure B-1. Forward-Scattered Reradiation Patterns From Aircraft and Ships. The bistatic properties of metal objects are illustrated for aircraft and ships. The bold arrows shown around the perimeter of the figure denote the infinite number of directions from which the incident microwave waveform may arrive to excite the metal objects. In this concept, the impedance at the phase center of the antenna transfers power (heat) in the incident wavefront that excites the facets of the metal structures. The axes of the reradiation patterns are directed toward a cooler media than the impedance at the phase center, id est, the Cosmic Background, either directly or after a reflection from the sea. The microwave power flow and the reradiated lobe patterns all conform in their direction to the Second Law of Thermodynamics. The reradiation patterns propagate toward the Cosmic Background over a solid angle of $2-\pi$ steradians. The reradiation patterns are formed from the current wavelets that originate from point sources (current maxima) of radiation. The lobes of the reradiation patterns are formed by the diffraction and interference patterns of the wavelets that originate from the point sources (current maxima). The reradiation from the metal objects is produced by the Kirchoff-Huygens Principle of reradiation.

where

k = Boltzman Constant, in joules.

T_{pc} = Thermodynamic temperature of the impedance at the phase center of the antenna, 290 kelvins for this example.

T_{Cos} = Blackbody temperature of the Cosmic Background (2.7 kelvins at microwave wavelengths).

B_n = Noise bandwidth of the predetection filter in the receiver. A noise bandwidth of 100 megahertz is adopted for the examples given in this monograph.

The thermodynamic temperature of the impedance at the phase center of the antenna, T_{pc}, is in thermal equilibrium with the instantaneous field of view (scene)[3] that is contained within the principal lobe of the antenna pattern. By reciprocity, the gain function of the antenna causes the impedance of the phase center to maintain a state of thermal equilibrium with the scene; this is a necessary condition that is explained by the Zeroth Law of Thermodynamics.[1]

By substitution of the modeled quantities into equation (B-1),

$$P_{av} = (1.380662 \times 10^{-23})\ (290 - 2.7)\ (10^{8})$$

$$= 397 \times 10^{-15} \text{ watts, or 397 femtowatts}$$

The structure of equation (B-1) shows that for the assumed thermodynamic temperatures of the impedance at the phase center of the antenna and the Cosmic Background, the available power (heat) flow will occur from the phase center of the antenna to the Cosmic Background through the gain function of the antenna and through the intermediary bistatic scattering properties of the projected area of the aircraft. The direction of the flow of microwave power is controlled by the Second Law of Thermodynamics, and the direction of

the power flow is irreversible. The incident power that impinges upon the metal surfaces of the aircraft is collected by the scattering surfaces of the projected area. By the Kirchhoff-Huygens Principle of reradiation from metal objects, the reradiated power will be directed, ultimately, to the Cosmic Background.

The facets on the metal surfaces of the aircraft comprise its projected area and produce gain in the direction of the phase center of the antenna. The facets of the surfaces of the projected area of the aircraft that reradiate toward the Cosmic Background similarly possess gain. It is the combined gains of the antenna and the incident and forward-scattered gain of the aircraft that produce the system conditions that will result in a feasible detection, as we will see in the mathematical developments that follow.

At this juncture, we are reminded that the noise level in the predetection noise bandwidth of the receiver--whose input terminals are connected to the phase center of the antenna--is 1.38 femtowatts, given that the receiver has a temperature resolution of 1 kelvin. That is,

$$P = k\, T_{res}\, B_n, \quad \text{in watts} \tag{B-2}$$

where

k = Boltzmann Constant, in joules.

T_{res} = Temperature resolution of the receiver, in kelvins.

B_n = Predetection bandwidth of the receiver, 100 megahertz.

The ratio of the available power from a natural source to the predetection noise-power-level in the receiver is expressed by

$$P_{ratio} = 397/1.38 = 288, \quad \text{or} \quad 25 \text{ dB}$$

The power that is transferred from the impedance at the phase center of the antenna to the Cosmic Background is construed to be the signal power, P_s. The change in the power level across the phase-center impedance is detected by the receiver at its input terminals.

Before proceeding with the development of the system transfer equations that will ultimately explain the detection of the CV-990/B-707 aircraft, it is relevant to discuss the elements of the detection process itself. The source of the available microwave power is the difference in the thermodynamic temperatures existing between the scene and the Cosmic Background as it is shown in expression (B-1). The magnitude of the available power (heat) may be reckoned in femtowatts when the difference temperatures are modified by the Boltzmann Constant and the predetection bandwidth of the receiver. Expression (B-1) is recognized as the microwave approximation to the general Planckian Equation which explains the general properties of blackbody radiation. The development of equation (B-1) is given in many places in the contemporary technical literature (see References [2] and [7]).

In principle, the integrated thermodynamic-scene temperature operates functionally as the primitive source of microwave energy (which is also construed as heat) that powers the detection process.

Before the metal object intrudes into the pale of the scene, the impedance at the phase center of the antenna and the scene are maintained in a continual state of thermal equilibrium by the principle of the Zeroth Law of Thermodynamics. The thermodynamic temperatures of the impedance at the phase center of the antenna and the scene itself are inextricably affected by the reciprocity principle that is implicit in the antenna gain function. The properties of the scene are explained and defined in Footnote 3 where, operationally, the scene is also called the instantaneous field of view (IFOV).

When a metal object intrudes into the scene, the impedance at the phase center of the antenna transfers heat to the Cosmic Background through the gain function of the antenna and through the incident and forward scatter gains of the metal object. The direction of the heat flow is controlled by the Second Law of Thermodynamics.

During the time that the metal object exists within the pale of the scene, the state of thermal equilibrium is modified, id est, the impedance at the phase center of the antenna radiates its heat to the Cosmic Background through the antenna gain function and through the incident and forward gains of the metal object.

The radiant emittances of the media, contained within the pale of the scene, continually operate to reestablish a state of thermal equilibrium with the impedance at the phase center of the antenna. The input terminals of the receiver are connected across the impedance at the phase center of the antenna. The thermodynamic temperature variations of the impedance at the phase center report the intrusion of the metal object into the pale of the scene and determine the statistical properties of the aircraft detection.

Having discussed and defined the basic concepts, principles, and considerations that affect detection of metal objects, let us now proceed to structure the microwave system transmission equations that will allow us to compute

- Signal-to-clutter ratio.
- Allowable false-alarm-rate.
- Probability of detection.

The observing mode for which the microwave transmission equations are modeled is keyed to the application of a thermodynamic sensor as it is applied in an imaging mode (see Figure 5). The imaging mode is important because it is construed as a searching process that deals with the basic detection processes of a metal object that exists within the pale of a scene. Once the detection is accomplished, the imager reports the scene location of the metal object and it continues on its programmed search for other objects.

The guiding and paramount consideration of this monograph is to determine the detection criteria for metal and emitting objects from geostationary orbit where it is perceived that the sensors are operating in a programmed search mode, as is illustrated in Figure 5.

The transport of microwave power, P_s, from the impedance at the phase center of the antenna to the metal object and thence to the Cosmic Background is written as follows:

$$P_s = P_{av}(A_c \eta) \frac{1}{4\pi R_s^2} G_i G_f, \quad \text{in watts/hertz} \tag{B-3}$$

where P_{av} is the available power as given by

$$P_{av} = k(T_{pc} - T'_{CB}), \quad \text{in watts/hertz}$$

and where

k = Boltzmann Constant, in joules.

T_{pc} = Thermodynamic temperature of the impedance at the phase center of the antenna.

T'_{CB} = The blackbody temperature of the Cosmic Background where it is increased by the emission from gases and water particulates in a planetary atmosphere. The blackbody temperature of the Cosmic Background and the thermodynamic temperatures of atmospheric gases are properly combined in a thermodynamic temperature transfer equation and the result is expressed in units of kelvins.

A_c = Area of the collecting aperture, in meters^2.

η = Solid-angle main-beam efficiency, a dimensionless quantity. The solid-angle main-beam efficiency is abundantly treated and defined in the contemporary technical literature, exempli gratia, Reference [4]. The parameter is not to be confused with antenna efficiency that is typically applied to radar and communications antennas.

R_s = Slant range, in meters.

G_i = Gain of the collecting area (facets) on the metal object that intercepts the power density in the arriving wavefront (incident) from the impedance at the phase center of the antenna, a dimensionless quantity.

G_f = Gain of the forward scattered wavefront from all of the facets on the metal object, a dimensionless quantity.

The terms G_i and G_f are applied more usefully in equation (B-3), where they are expressed in terms of their respective collecting and forward-scattered areas. Id est,

$$G_i = 4\pi A_i/\lambda^2$$

$$G_f = 4\pi A_f/\lambda^2$$

where λ symbolizes the operating wavelength of the microwave sensing system, and A_i and A_f are the collecting and forward scattering areas of the facets on the metal object, respectively. The area A_i intercepts the wavefront that arrives from the phase center of the antenna. The area A_f reradiates the power intercepted by A_i by the Kirchhoff-Huygens Principle. Because A_i and A_f involve different scattering centers on the metal target, they are construed to be uncorrelated (decorrelated in the statistical sense). Because the collecting area and the forward scatter areas are significantly uncorrelated and, therefore, operate independently, the corresponding gains that are formed from these respective areas are also uncorrelated and are construed as independent parameters.

Now

$$G_i = \frac{4\pi A_i}{\lambda^2} \quad \text{and} \quad G_f = \frac{4\pi A_f}{\lambda^2}$$

For modeling purposes, let

$$A_i = A_f = A_t$$

where A_t represents the expected value of the projected cross section of the metal object. Implicit in A_t is the expectation that the metal object possesses statistical scattering properties that are construed as bistatic properties.

Then

$$G_i G_f = \frac{(4\pi A_t)^2}{\lambda^2}$$

which, when recast into a more perspicuous form, becomes

$$G_i G_f = \frac{(4\pi)^2 A_t^2}{\lambda^4} \qquad \text{(B-4)}$$

The rationale and the mathematical development of (B-4) are very profound; they show that the power transfer from the phase center of the antenna to the Cosmic Background has a λ^4 dependency.

When the relative roughness of the surfaces of the metal facets on the metal object are smooth compared to the operating wavelength, the S/C ratio will possess a λ^4 dependency from $G_i G_f$. The fourth power exponent suggests that smaller collecting apertures will produce satisfactory S/C ratios. From this consideration, great economies may be realized in the manufacture of the antenna structure.

By substituting equation (B-4) into (B-3) and by recasting and collecting terms, we obtain

$$P_s = \frac{4\pi\, k(T_{pc} - T'_{CB})\ (A_c\ \eta)\ (A_t\ Z_r \cos\theta_i)^2}{R_s^2\ \lambda^4}, \quad \text{in watts/hertz} \tag{B-5}$$

The terms Z_r and θ_i are also introduced into (B-5). They are defined in Appendix A for the short-pulse-radar case. Basically, Z_r specifies the fraction of the projected area of the metal object, A_t, that participates in producing bistatic gain. Empirical estimates of Z_r for aircraft targets, where the monostatic backscattering is from the front of the aircraft, is 6%.

The angle of incidence, θ_i, is introduced into equation (B-5) to modify the projected target area as it is viewed from the aspect of the sensor in geostationary orbit. At a latitude of 55 degrees, θ equals 57 degrees (see Table 1). Near the equator, the angle of incidence approaches normal incidence.

The expected value of the S/C ratio for the detection of the metal object is expressed by

$$\frac{S}{C} = \frac{P_s}{P_n}$$

where

$$P_n = k\ T', \quad \text{in watts/hertz} \tag{B-6}$$

where

k = Boltzmann Constant

$$T' = \left(T_{res}^2 + T_{clut}^2 \right)^{1/2}, \quad \text{in kelvins} \tag{B-7}$$

The parameter T' is derived from the orthogonal average (root sum of squares) of the temperature resolution of the receiver T_{res} with the clutter temperature variations that occur during the search mode. The symbol T_{clut} is the clutter-temperature component of T'. In Reference [5], clutter-temperature estimates are commonly observed at 0.45 kelvins for a quiet sea at an operating wavelength of 8 millimeters.

Expression (B-7) shows that P_n contains both the system noise of the receiver and the clutter power that is produced by scanning the collecting aperture. The mechanisms that produce clutter power in microwave imagers are limned in References [5] and [6].

The S/C ratio is computed from the ratio P_s/P_n by combining expressions (B-5) and (B-6) and by introducing T' from (B-7). Therefore,

$$\frac{\hat{S}}{C} = \frac{4\pi(T_{pc} - T'_{CB})(A_c\ \eta)(A_t\ Z_r\ \cos\theta_i)^2}{R^2\ \lambda^4\ T'}, \quad \text{a dimensionless quantity} \tag{B-8}$$

where the expression (B-8) is construed to be a general, closed-form expression for the expected value of the S/C ratio for metal objects.

For the case of a thermodynamic sensor that is disposed in geostationary orbit, let us compute the expected value of the S/C ratio for a CV-990/B-707 type of aircraft, from (B-8), where the aircraft is viewed against a sea background on a clear day.

Figures A-3 and A-4 illustrate a thermodynamic model of the atmospheric and surface losses where they are construed to be the thermodynamic temperature of the scene (IFOV).

The aircraft is disposed at an altitude above the planet where the atmospheric losses are regarded as negligible.

The following parameter values will be substituted into expression (B-8):

T_{pc} = The temperature of the impedance at the phase center of the antenna, 129 kelvins (from Figure A-4).

T'_{CB} = Blackbody temperature of the Cosmic Background, 2.7 kelvins.

A_c = Area of the collecting aperture, 730 meters^2.

η = Solid-angle main-beam efficiency of the antenna, 0.95.

A_t = Projected area of the aircraft as viewed from normal incidence, 382 meters^2.

Z_r = Reflectivity factor where it is construed as the fraction of the facets in A_c that participate as bistatic scatterers, 0.06. In the argot of the radar art, Z_r is regarded as the monostatic backscatter coefficient. Typically, it is assigned a numerical value of -12 dB below 1 meter^2.

θ_i = Angle of incidence from which the projected area of the aircraft, A_t, is viewed. The projected area of the aircraft (at normal incidence) is diminished by the cosine of the incidence angle, 57 degrees, as it is here viewed from geostationary orbit.

R_s = Slant range to 55 degrees latitude, 38,288 kilometers.

λ = Operating wavelength of the thermodynamic sensor, 0.008108 meters.

T' = Orthogonal average of the receiver noise temperature and the thermodynamic temperature of the clutter. Given that the temperature resolution of the receiver is 1 kelvin and that the clutter temperature is 0.45 kelvins, then $T' = 1.10$.

By substitution of the parameter values given above in expression (B-8) for the detection of the CV-990/B-707 aircraft from geostationary orbit, we obtain

$$\frac{\hat{S}}{C} = 24.61, \text{ or } 13.91 \text{ dB},$$

which is reasoned to produce a high confidence detection, but it falls somewhat short of the desired +15 dB criterion for high precision and accuracy in the measurement.

C-2

B.1 PROBABILITY OF DETECTION OF THE CV-990/B-707 AIRCRAFT

The probability of detection of the CV-990/B-707 aircraft is controlled by the statistical parameters produced by the imager mode, as described in Figure 5.

Suppose it is determined that on an operational basis, one false alarm in every 60 seconds is allowable. From the imager pattern shown in Figure 5 there are 100 independent measurements performed every 3 seconds in the swath, which is, equivalently, 2,000 independent observations every 60 seconds.

From this model, the false alarm probability, P_N, is expressed by

$$P_N = \frac{\text{Number of allowable false alarms}}{\text{Number of independent samples that occur during the false alarm time}}$$

which, in this model as it is keyed to Figure 5, and allowing for 1 false alarm every 60 seconds, yields

$$P_N = 1/2000 = 4 \times 10^{-4}$$

From Reference [3], the probability of detection for a nonscintillating metal object is expressed by

$$P_d = P_N^{[1/(1+S/C)]} \qquad \text{(B-9)}$$

which, by substitution of the numerical entries derived above for the CV-990/B-707 type of aircraft as it is perceived to operate in the microwave imager mode, shown in Figure 5, from geostationary orbit, yields

$$P_d = 0.74 \quad \text{or} \quad 74\%$$

The statistical interpretation of the probability of detection (expression B-9), as it is structured here, conforms with the expectation that 7 out of 10 CV-990/B-707 type of aircraft that occur within the imaged area (Figure 5) will be detected. Detection occurs when the change in the thermodynamic temperature of the impedance at the phase center of the antenna exceeds the threshold level set for the detector. The corollary of detection is false alarm--which, in this example, and by expectation, will occur once every 60 seconds.

The conclusions and commentary that are concerned with the detection of the CV-990/B-707 aircraft are epitomized in Section 5.2.1.

B.2 DETECTION OF A METAL BUOY

The seas of the planet are generously endowed with metal buoys that serve to sense the local environment of the sea. Buoys are frequently moored on the continental shelves around land masses, and others drift (by design) with the prevailing ocean currents. The principal function of the buoys is to monitor meteorological quantities and sea-surface conditions and to report the measurements to data repositories via satellite transmission links.

Buoys are important: they measure and report

- o Sea-surface temperature.
- o Wind speed and direction at the sea surface.
- o Pressure.
- o Air temperature.

sometimes on an hourly schedule.

Buoys are constructed in rectangular and discoid shapes. Their physical dimensions range from about 6 to 12 meters. Towers are affixed to the buoys that support some of the meteorological sensors. The largest buoys are discoid types that are 12 meters in diameter with an exposed metal surface area of 113.1 meters^2.

Within the context of this monograph, buoys are perceived as detectable metal objects whose geodetic coordinates are precisely known and whose physical shapes and areas are well defined. For operational geostationary microwave imagers, buoys serve as test objects to verify detection capability. A photograph of a 12-meter-diameter moored metal buoy is shown in Figure B-2. The bistatic properties of a metal buoy are illustrated in Figure B-3.

It is introspective and interesting to investigate the detection of a metal buoy with a thermodynamic sensor from the distance of geostationary orbit. To this end, we choose to analyze the detection of the metal buoy

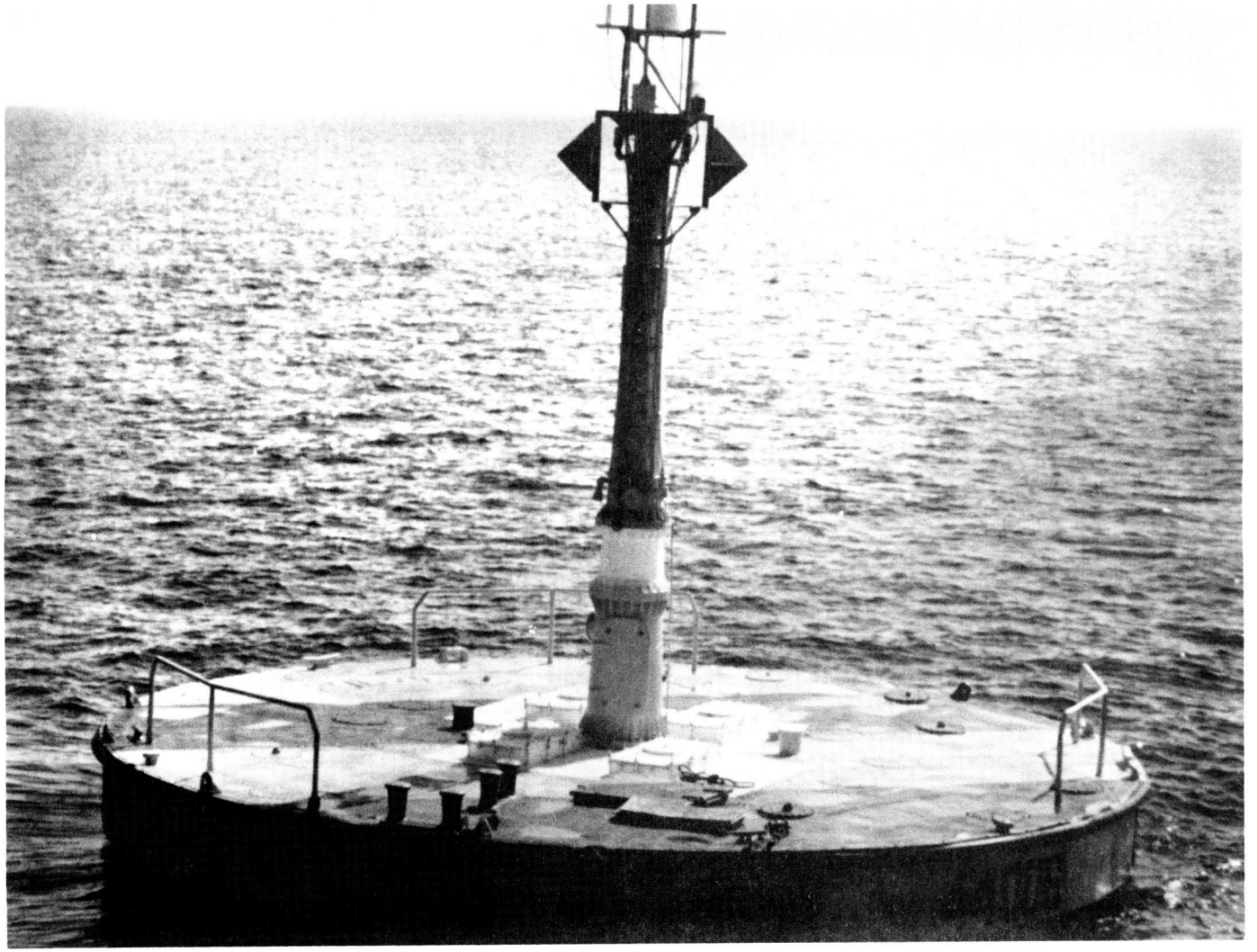

Figure B-2. Metal Buoy. Illustrated in this figure is a 12-meter-diameter moored, discus-type metal buoy. The area of the discoid figure contains 113.1 meters^2. The vertical column serves as a support platform for meteorological sensors. Near the top of the vertical column are two corner reflectors for the purpose of enhancing the radar cross section of the buoy. The miscellaneous fittings, mooring posts, and metal plates are, by expectation, rough on the scale of 8-millimeters wavelength.

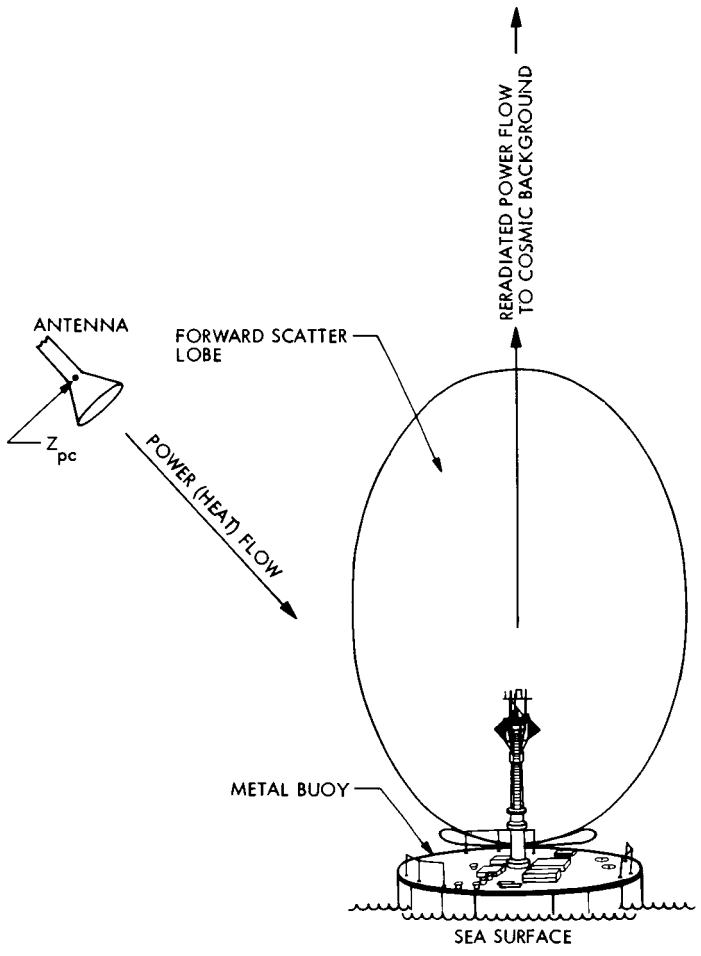

Figure B-3. Bistatic Properties of a Metal Buoy. The bistatic properties of a metal buoy are illustrated in this figure. When the power density in an incident wavefront illuminates the discoid figure of the buoy, a large central reradiation-lobe is produced through the vertical axis of the discoid. Tertiary lobes are also formed about the central lobe, as shown.

The flow of microwave power (heat) from the impedance at the phase center of the antenna is intercepted by the metal surfaces of the buoy and is <u>reradiated</u> (not reflected) toward the Cosmic Background through the lobe structure, which is construed as forward scatter. The metal surfaces (facets) of the buoy structure that intercept the incident wavefront that arrives from Z_{pc} are independent (uncorrelated) with the facets that participate to form the reradiation lobe structure that is directed toward the Cosmic Background. The power that is intercepted from Z_{pc} induces a pattern of currents that suffuses the entire buoy structure.

The current maxima operate as myriad point sources which individually produce radiated wavelets. By the processes of diffraction and interference, the wavelets produce the lobe structures as are shown in the figure. Notably, the direction of the reradiation pattern (lobes) are uncorrelated with the direction of arrival of the incident wavefront.

The transformation of the power density in the incident wavefront to the reradiated power in the forward scatter lobes is executed by the Kirchhoff-Huygens Principle [4].

- o At 55 degrees latitude.
- o On the equator near the nadiral point.

These latitudes are chosen because the detectability of the buoy is importantly affected by variations (differences) in

- o Slant range.
- o Aspect.
- o Path length through the planetary atmosphere.

The buoy is perceived as a metal object with bistatic reradiation properties and with detectability criteria that are similar to the CV-990/B-707 aircraft. From this, we choose to use Equation (B-5) in its exact form, as given above. The terms of Equation (B-5) will be modified as is appropriate to deal with the disposition of the metal buoy at a location of 55 degrees latitude and also near the nadiral point of the geostationary spacecraft.

The primary objective of these analyses is to calculate the S/C ratio of the buoy where it is construed as a detectable metal object that lies within the search pattern of the microwave imager as shown in Figure 5.

First we shall calculate the S/C ratio of the buoy where it is detected at 55 degrees latitude. Next we shall calculate the S/C ratio of the buoy where it is detected near the nadiral point of the geostationary spacecraft on the equator.

B.3 DETECTION OF A METAL BUOY AT 55 DEGREES LATITUDE

We choose to use the same microwave-imager equipment and operating wavelength as for the detection of the CV-990/B-707 aircraft. The mathematical expression that was derived for computing the S/C ratio for the CV-990/B-707 aircraft (Equation B-8) will be used for computing the S/C ratio for the metal buoy. For the example of the metal buoy, some new numerical values will be computed and substituted into (B-8).

Equation (B-8) requires two modifications of its terms for the metal buoy at 55 degrees latitude: T'_{CB}, the thermodynamic temperature of the Cosmic Background as it is modified by the attenuation of the planetary atmosphere; and A_t, the area of the metal object (the buoy). The mathematical expression that explains the thermodynamic temperature T'_{CB} for a metal object that is immersed in a planetary atmosphere is excerpted from Reference [4] and restated here as equation (B-10) without modification of its primitive terms:

$$T'_{CB} = \frac{T_{cos}}{L_{ad}\, L_{au}} + \frac{T_{ad}\,(L_{ad} - 1)}{L_{ad}\, L_{au}} + \frac{T_{au}(L_{au} - 1)}{L_{au}}, \quad \text{in kelvins} \tag{B-10}$$

where

L_{ad} = Attenuation in the slant path through the planetary atmosphere between the Cosmic Background and the buoy. The parameter L_{ad} is expressed either as a decibel quantity or, equivalently as it is here, as a number greater than 1. Exempli gratia, a 1 dB loss may be expressed as an exponent of 10 and as a number greater than 1 by

$$10^{1/10} = 1.26$$

L_{au} = Attenuation in the slant path between the collecting aperture and buoy, where the attenuation is expressed as a number greater than 1.

T_{ad} = Integrated physical temperature of the atmosphere intervening between the Cosmic Background and the buoy, typically modeled at 280 kelvins.

T_{au} = Integrated physical temperature of the atmosphere intervening between the collecting aperture and the metal object, typically modeled at 280 kelvins.

The three terms expressed by equation (B-10) express the thermodynamic temperature contributions to T'_{CB}, <u>id est</u>,

T'_{CB} = (Cosmic Background) + (Cosmic Background to buoy) + (collecting aperture to buoy), in kelvins

when

$T_{ad} = T_{au} = 280.$

L_{ad} = 1.054, the water vapor and oxygen losses through the total atmosphere in the zenith path on a clear day, 0.23 dB.

L_{au} = 1.084, the water vapor and oxygen losses through the total atmospheric path at an angle of incidence of 57 degrees on a clear day, 0.35 dB.

By substitution of the modeled-term values into expression (B-10), we obtain

$$T'_{CB} = \frac{(2.7)}{(1.054)(1.084)} + \frac{280\ (1.054 - 1)}{(1.054)\ (1.084)} + \frac{(280)\ [(1.084) - 1)]}{(1.084)}, \quad \text{in kelvins}$$

$$= 2.36 + 13.95 + 21.7$$

$$= 38 \text{ kelvins}$$

Substituting the numerically derived values for T'_{CB} (38 kelvins) and A_t (113.1 meters^2) for the area of the buoy and solving for the expected value of the S/C ratio in (B-10)

$$\frac{\hat{S}}{C} = \frac{4\pi\,(129 - 38)\,(730 \times 0.95)(113 \times 0.06 \times \cos 57)^2}{(38{,}288 \times 10^3)^2\,(0.008108)^4\,(1.1)}$$

$$= 1.55, \text{ or } 1.92 \text{ dB}$$

where

T_{pc} = 129 kelvins, the thermodynamic temperature of the impedance at the phase center of the antenna on a clear day (also the scene temperature). Derived in Figure A-4.

A_c = 730 meters^2, the area of the collecting aperture.

η = 0.95, the solid-angle main-beam efficiency of the collecting aperture.

A_t = 113.1 meters^2, the area of the discoid figure of the buoy (12-meter-diameter).

Z_r = 0.06, the reflectivity factor expressing the fraction of the area of the target that participates in the bistatic propagation properties of the buoy.

θ_i = 57 degrees, the angle of incidence at 55 degrees latitude. θ_i expresses the reduction in the area of the buoy because of the aspect angle from which it is viewed by the thermodynamic sensor on the spacecraft.

R_s = Slant range, in meters.

λ = Operating wavelength, in meters.

T' = 1.1 kelvins, the orthogonal average (root sum of squares) of the clutter temperature (0.45 kelvins) and the temperature resolution (1 kelvin).

The results of the solution of equation (B-8) for the buoy at 55 degrees latitude are epitomized and discussed in Section 5.2.2.1.

B.4 DETECTION OF A BUOY NEAR THE NADIRAL POINT OF THE SATELLITE ON THE EQUATOR

It is interesting to compute the expected value of the S/C ratio for the case where the buoy is located on the equator and near the nadiral point of the geostationary satellite. For this case the T'_{CB} is reduced, because the path length through the atmosphere is decreased. Also, and most importantly, the angle of incidence, θ_i, reduces to a numerical value of 1, because it is a nadiral-path measurement. In addition, the slant range, R_s, reduces to the altitude of the geostationary satellite. These factors, operating in consonance, significantly improve the expected value of the S/C ratio.

A new value of T'_{CB} is computed for the case here where the propagation paths to and from the buoy pass through the nadir.

Again we solve for T' for the case where the attenuation through the atmosphere is the same for L_{ad} and L_{au}. The zenith path attenuation is given as 0.23 dB, or, equivalently, when expressed as a number greater than 1, 1.054.

Returning to solve for T'_{CB} from equation (B-10), we obtain, by substitution,

$$T'_{CB} = \frac{2.7}{(1.054)(1.054)} + \frac{280\ (1.054 - 1)}{(1.054)(1.054)} + \frac{(280)\ [(1.054) - 1)]}{(1.054)}, \quad \text{in kelvins}$$

$$= 31.12 \text{ kelvins}$$

which, when substituted into equation (B-8) for the same conditions as for the metal buoy at 55 degrees latitude, results in

$$\frac{\hat{S}}{C} = \frac{4\pi\ (129 - 31)[(720)(0.95)][(113)(0.06)(\cos\ 0)]^2}{(35{,}760 \times 10^3)^2\ (0.008108)^4\ (1.1)}$$

$$= 6.37 \text{ or } 8.04 \text{ dB}$$

Based on the search pattern described in Figure 5, the probability of detection is expressed by substituting $\frac{S}{C}$ into equation (B-9), where the false alarm rate, P_N, is 4×10^{-4}, as follows:

$$P_d = (4 \times 10^{-4})^{[1/(1+6.37)]}$$

$$= 0.35$$

where the proper interpretation of P_d expresses the expectation that three metal buoys (12-meter-diameter) out of 10 will be detected at the equator near the nadiral point of the geostationary satellite.

The results of the solution to equation (B-8) for a buoy that is located on the equator and near the nadiral point of the geostationary satellite are epitomized and discussed in Section 5.2.2.2.

B.5 DETECTION OF SHIPS FROM GEOSTATIONARY ORBIT

It is well known in radar theory, and in the applied practice, that the monostatic and forward scattering cross sections of ships are a very complex phenomenon. The intricate mechanical structures of ships produce a myriad of electromagnetic scattering centers from the metal facets which operate both as collecting areas and as point sources of reradiation.

Sometimes the scattering centers operate in consonance and produce lobe patterns whose central axes possess the properties of high gain. Sometimes the scattering centers operate in dissonance and produce interferences that are perceived as nulls in the reradiation pattern. Because of the quasi-random orientations of the metal facets on the ship's structure, the backscattering cross sections (monostatic) and the forward scattering cross sections are critically dependent upon the aspect angle of the illuminating wavefront.

Whenever the metal facets of the ship are excited by an incident wavefront, a myriad of creeping currents suffuse the ship and produce a characteristic reradiation pattern that is disposed over a solid angle of 2π steradians. The facets that collect the incident waveform and the facets that form the radiating surfaces of the reradiated pattern are patently independent, and for this reason the incident and the reradiated patterns are construed as decorrelated.

The property of a metal object (such as a ship) whose facets collect microwave power from an arbitrary incident wavefront and thereafter reradiate the power (albeit with some loss) through an independent system of reradiation elements is defined as a bistatic scatterer. The aspect angle over which the incident waveform arrives critically affects the magnitude of the collected power.

Ships expose large collecting and reradiating surfaces, especially at their broadsides, and to a lesser degree at the bow and stern aspects. From geostationary orbit, and at 55 degrees latitude, the angle of incidence

is 57 degrees, which ensures that the ship structure is viewed favorably (nearly normal) to its broadside and to the bow and stern. At 55 degrees latitude, it is not geometrically possible to view ships at their zenith aspect.

When the power density in an incident wavefront illuminates a ship's structure, from any aspect, a forward scattered lobe structure is produced at and near the zenith path, which, in turn, operates to transport power (heat) to the Cosmic Background.

When a metal ship structure is illuminated by a wavefront that arrives from any direction, the metal facets on the structure operate in consonance to produce a reradiation pattern in the forward direction that encompasses a solid angle of 2π steradians. The reradiation pattern is formed by the Kirchhoff-Huygens Principle [4] of reradiation from the myriad point sources that produce wavelets and ultimately form diffraction and interference patterns in the forward scattered direction--all of which are intercepted by the Cosmic Background.

One thing that deserves consideration is the fact that large metal ships--men of war, for example--produce large scattering cross sections that are far greater than for aircraft, exempli gratia, CV-990/B-707, and for this reason alone produce larger S/C ratios and probabilities of detection.

Some observational comparisons among aircraft and ships deserve consideration: ships are immersed in the attenuating layers of the atmosphere; high-altitude aircraft are not. Cloudforms always exist as an attenuating media that affect ship detectability. For aircraft, detectability depends upon the character of the cloudforms and the altitude of the aircraft.

It is interesting and informative to investigate the detectability of ships from geostationary orbit. Let us consider two candidate types for investigation:

The research vessel that is illustrated in Figure B-4 characterizes the involute physical structure of a large number of ships. It is, in fact, a

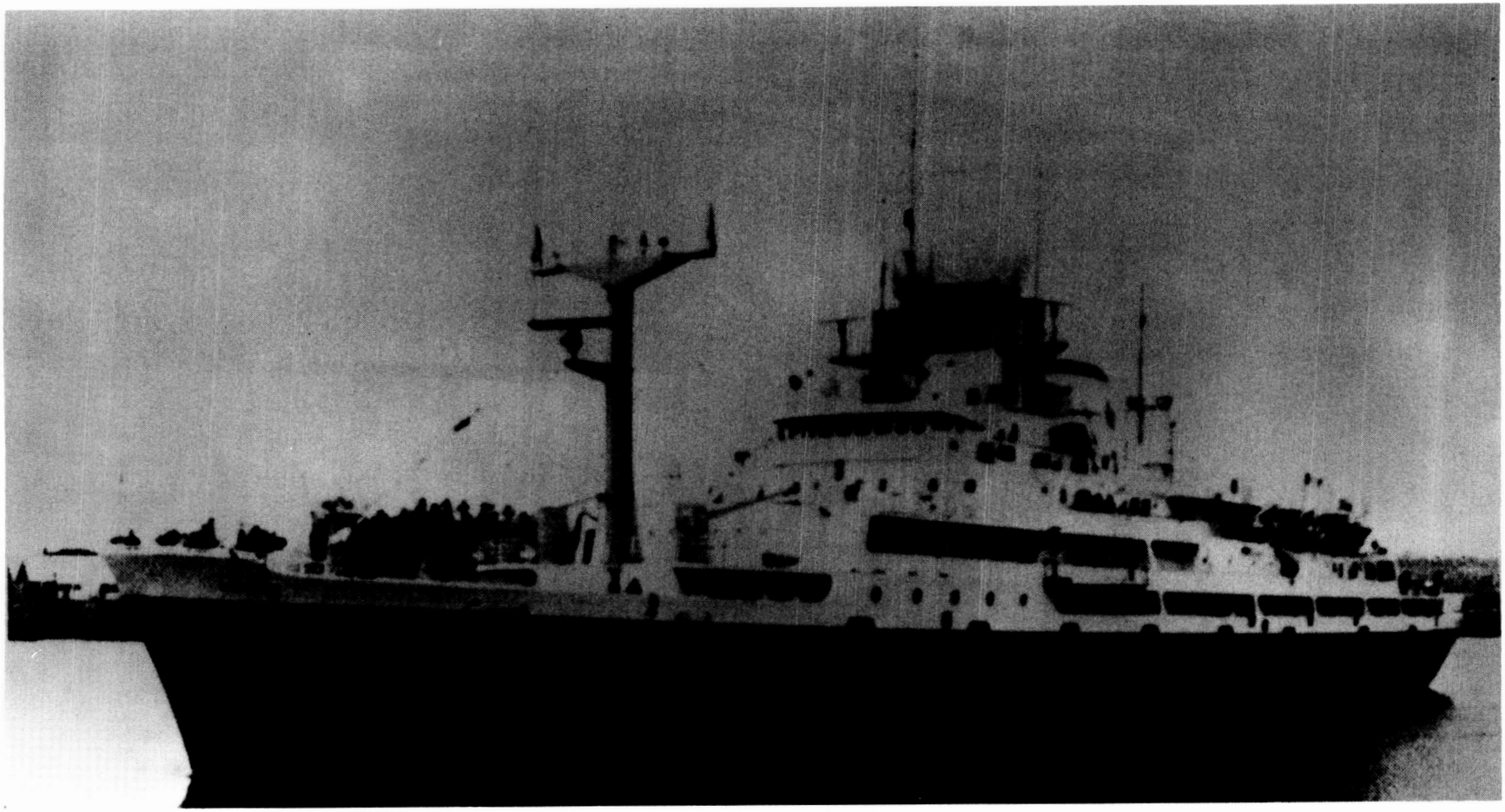

Figure B-4. A Type of Ship's Structure That Exhibits Extremely Complex Monostatic and Bistatic Properties

very common type of ship that is patently similar to certain classes of freighters, frigates, destroyers, and cruisers. The monostatic backscattering properties of these vessels are determined almost entirely by taking actual backscatter measurements on antenna ranges and by employing fractional-scale models of the ship's structure. Estimating the monostatic (and bistatic) properties of ships from the dispositions of the facets in their metal structures is reasoned to be a seemingly intractable problem that is surely fraught with enormous technical difficulties.

By comparison, however, the regular and predictable surfaces of the aircraft carrier, as shown in Figure B-5, is readily adaptable for modeling purposes, provided that the accuracy expectations of their monostatic and bistatic scattering cross sections are loosely specified.

The geometrical figure of the aircraft carrier may be described conceptually as an imperfect rectangular prism that rests on the sea surface. The bistatic properties of the rectangular prism are patently similar to those of the metal buoy as shown in Figures B-2 and B-3; that is, the incident microwave wavefront illuminates the metal facets that are disposed on the metal deck of the aircraft carrier, which produce a reradiation pattern that forms a large forward-scattered major lobe in the zenith direction. Numerous tertiary lobes are also formed about the major lobe whose axes are directed toward arbitrary pointing positions over the solid-angle of 2π steradians. The reradiation, or forward scattered pattern, is produced by the Kirchhoff-Huygens Principle of reradiation.

Because the figure of the aircraft carrier exhibits a patently useful degree of symmetry, the aircraft carrier is perceived as an adaptable and interesting metal object from which to estimate its bistatic gain properties from the total surface area of the metal decking, recognizing, of course, that the sides of the ship contribute to, and affect, the bistatic gain patterns. For this model, however, we choose to simplify the analysis and will ignore the areal contributions from the sides of the ship.

Figure B-5. The Aircraft Carrier U.S.S. Saratoga. This figure illustrates the regular geometrical properties of the U.S.S. Saratoga which produce bistatic scattering properties that are characterized by high forward-scattered gain. The geometrical figure of the aircraft carrier approximates a rectangular prism with areal contributions to the scattering cross sections from both the metal deck and from the sides. Certain classes of large aircraft carriers are 329 meters long and 82.5 meters wide. Their projected bistatic scattering cross section (area), as viewed from normal incidence, is 27,071 meters^2 (6.6 acres). An incident microwave wavefront on the carrier, which arrives from any direction, will produce, by the Kirchhoff-Huygens Principle of reradiation, a large forward-scattered lobe that exhibits extremely high gain in the direction of the zenith.

Given the projected area of the deck surfaces, as viewed from geostationary orbit, it is interesting and informative to calculate the S/C ratio and the probability of detection from the general expression for metal objects in Equation (B-8). Given also that the aircraft carrier may be of the U.S.S. Constellation class, with a length of 329 meters and with a nominal width of 82 meters (26,978 meters^2), let us compute the S/C ratio and the probability of detection as viewed by a thermodynamic sensor that is carried by a satellite vehicle in geostationary orbit.

By substituting the appropriate aircraft-carrier parameters into equation (B-8), and by further assuming that the same observing equipment is used as for the detection of the metal buoy, on a clear day, and at 55 degrees latitude, we obtain

$$\frac{\hat{S}}{C} = \frac{4\pi\,(129 - 38)[(730)(0.95)][(26{,}978)(0.06)(\cos 57)]^2}{(38{,}288 \times 10^3)^2\,(0.008108)^4\,(1.1)},$$

a dimensionless quantity derived by substitution in (B-8)

$= 88{,}443.16$ as a numerical ratio, or, equivalently, 49.5 dB

Using equation (B-9), the probability of detecting the aircraft carrier can be computed from the S/C ratio.

Assuming that the search pattern is applied to the observation of the aircraft carrier, as shown in Figure 5, and for the same false alarm rate that was used for the detection of the metal buoy ($P_N = (4 \times 10^{-4})^{[1/(1+88{,}443.16)]}$), we obtain

$$P_d = (4 \times 10^{-4})^{[1/(1+88{,}443.16)]}$$

$$= > 0.99$$

The results of the above computation for the expected value of the S/C ratio and for the probability of detection are epitomized in Section 5.2 with the CV-990/B-707 aircraft and the metal buoy.

APPENDIX C

THERMODYNAMIC OBSERVATION OF A COLD EDDY

Cold areas continually appear and evanesce from the surfaces of the seas. Generally, they display a circular pattern, but often they are quite irregular. The diameters of cold areas may range from a few kilometers to over a hundred kilometers. Besides being colder than the surrounding seawater--by one or two kelvins--the actual surface areas also tend to be smoother. The occurrence of some cold areas can be plausibly explained; others cannot.

The terminology assigned to cold spots varies somewhat depending upon the locality where they occur. On the south side of the Gulf Stream, in the western North Atlantic, near Cape Hatteras, "cold rings" or "cold eddies" move in the direction counter to the bore of the Gulf Stream. Cold eddies are created by frigid waters, moving southward from Newfoundland and Greenland, that are "pinched off" from the meandering bore of the Gulf Stream.

Cold rings are bona fide eddies, in an oceanographic sense, because they rotate with circular or spiral structure as they move laterally through the sea. Typically, the structures of cold eddies penetrate the depth of the sea to the extent of thousands of meters. Rarely do their thermometric temperature differences with respect to the surrounding sea exceed one or two kelvins. Cold eddies near the Gulf Stream exhibit lifetimes that range from months to years as they continually move westward on the south side of the Gulf Stream. Eventually, cold eddies break up and vanish as they approach the coast of the Carolinas.

A dedicated community of oceanographic researchers continually observes the sea surface for manifestations of cold eddies aborning, particularly in the vicinity of the Gulf Stream. Observations are conducted with satellite-borne sensors that operate in the visible and infrared wavelength region. However, visible and infrared wavelengths are poorly adapted to the task of sea surface observations because of their propagation limitations caused by persisting cloudforms.

Cold upwellings (as distinct from eddies) also appear on the surface of the sea. Upwellings are manifested as irregular cold areas that occur more abundantly in some regions of the sea than in others. Upwellings are common near Bermuda and also, albeit surprisingly, on and near the equator. The morphogenesis and morphology of cold upwellings are considerably different from the cold eddies near the Gulf Stream--and their causes are more conjectural.

Upwellings near the Island of Bermuda, for example, are believed to be caused by cold currents that move along the bottom of the sea. When a cold current encounters an obstruction on the floor of the sea, or a seamount, or a physically rising object of any description, the current is deflected upward to the surface, where it is manifested as a cold smooth area, au fond, an upwelling.

The extremely cold surface currents that circumvolve the Anarctic Continent operate to produce cold upwellings on the sea surface, mainly in the southern hemisphere, but even as far north as the equator, and more. What actually happens is that the cold, dense seawater that is contained in the Antarctic currents submerges below the warmer seawater to the north. The surface boundary where the cold water submerges is called the Antarctic Convergence Zone. The latitude of the convergence zone, for example, lies somewhere between New Zealand and Antarctica. Ultimately, the cold Antarctic seawater rises to the surface where it is manifested as a cold upwelling.

As they are perceived oceanographically, cold eddies and cold upwellings are interesting and useful objects: they contain information concerning the distribution and circulation of seawater on the planet.

From the coign of vantage of geostationary orbit, microwave receivers (where they are construed as thermodynamic sensors) are uniquely capable of detecting the occurrence of cold objects aborning and monitoring their seatracks throughout their lifetimes. Microwave wavelengths improve the detectability of cold objects through clouds and other particulate atmospheric

media. Cloud penetrability is especially important because cloudforms tend to increase in both their areal coverage and density with increasing latitude. To this extent, infrared and visible sensors are strongly disadvantaged.

It is illuminating, interesting, and perhaps useful to analyze the detectability of a cold eddy or upwelling by a thermodynamic sensor stationed in geostationary orbit.

Consider a cold eddy that has intruded into the instantaneous field of view (IFOV, or the scene) of the principal lobe of the antenna, as illustrated in the search pattern of Figure 5. It is given that the initial conditions of the observation show that the impedance at the phase center of the antenna, Z_{pc}, is in thermal equilibrium with the integrated radiant emittance of the scene. Further, the scene and Z_{pc} are in a state of thermal equilibrium as sustained by the reciprocity principle of gain in the antenna, and that thermal equilibrium is in conformance with the Zeroth Law of Thermodynamics.

Because, by definition, the eddy is colder than the mean thermodynamic temperature of the scene, microwave power (heat) will transfer from Z_{pc} to the projected collecting area of the eddy in conformance with the Second Law of Thermodynamics, <u>id est</u>, concisely stated, heat seeks cold.

The power density of the wavefront that is incident on the projected collecting area of the cold eddy is given by

$$P_{rce} = P_t G_t \frac{1}{4\pi R_s^2}, \quad \text{in watts/meter}^2$$

When the projected area of the eddy, A_{ce}, is entered into the expression for the case of normal incidence, we obtain

$$P_{rce} = P_t G_t \frac{1}{4\pi R_s^2} A_{ce}, \quad \text{in watts} \qquad \text{(C-1)}$$

where

$$P_t = k\,(T_{sc} - T'_{CB})\,B_n, \quad \text{in watts}$$

and where

k = Boltzmann Constant, in joules/hertz.

T_{sc} = Thermodynamic temperature of the scene, in kelvins (see Figure A-4).

T'_{CB} = Thermodynamic temperature of the transmission path included in the upwelling and downwelling paths through the atmosphere and with the Cosmic Background, in kelvins.

B_n = Predetection noise bandwidth of the receiver, in hertz.

and where the antenna gain is expressed as a function of its collecting area, A_c, and the solid-angle main-beam efficiency, η. Then

$$G_t = \frac{4\pi\,(A_c\,\eta)}{\lambda^2}, \quad \text{a dimensionless quantity}$$

The noise power contained with the predetection bandwidth of the receiver is given by

$$P_n = k\,T'\,B_n, \quad \text{in watts (C-2)}$$

where

T' = Orthogonal average (root sum of squares) of the temperature resolution of the receiver and the thermodynamic clutter temperature as it is an expected value from Figure 5.

Now the expected value of the S/C ratio is expressed by substituting the defined quantities above into (C-1) and (C-2) as follows:

$$\frac{P_{rce}}{P_n} = \frac{\hat{S}}{C} = \frac{(T_{sc} - T'_{CB})(A_c\ \eta)(A_{ce}\ \cos\theta_i)}{R_s^2\ \lambda^2\ T'}, \quad \text{a dimensionless quantity} \tag{C-3}$$

where it is noted that the cosine of the incidence angle, θ_i, is introduced into the equation to modify the projected area of cold eddy A_{ce} as a function of latitude.

The thermodynamic temperature of the transmission path from the phase center of the antenna to the Cosmic Background, through the upwelling and downwelling paths of the atmosphere, and including the thermodynamic properties of the cold eddy, is expressed in Figure A-3.

By rewriting the terms of Figure A-3, and by introducing the modeled assumptions for the properties of the cold eddy, we obtain

$$T'_{CB} = \frac{T_{cos}}{L_{ad}\ L_{surf}\ L_{au}} + \frac{T_{ad}\ (L_{ad} - 1)}{L_{ad}\ L_{surf}\ L_{au}} + \frac{T_{surf}\ (L_{surf} - 1)}{L_{surf}\ L_{au}} + \frac{T_{au}\ (L_{au} - 1)}{L_{au}}, \quad \text{in kelvins} \tag{C-4}$$

Now L_{surf} is defined as the loss in the cold eddy where it is expressed as a number greater than 1.

The reflectivity, ρ, of the collecting area, A_{ce}, is expressed by the fundamental thermodynamic expression

$$1 = \rho + \alpha + \varepsilon$$

where

α = Absorptivity

ε = Emissivity

from which L_{surf} is expressed by

$$L_{surf} = \frac{1}{1 - (\varepsilon + \alpha)} = \frac{1}{\rho}$$

Given that the cold eddy is observed on the surface of the sea at 55 degrees latitude and that the operating wavelength is at 8-millimeters wavelength on a clear day, and by substitution of the eddy parameters, we obtain

T_{surf} = Thermometric temperature of the collecting aperture formed by the cold eddy, 288 kelvins; based on a modeled assumption expressing the expectation that the thermometric temperature of the seawater in the surface of the eddy is 2 kelvins lower than the surrounding sea surface.

$(\varepsilon + \alpha)$ = The sum of the emissivity and the absorptivity, where the smooth, cold surface of eddy is assigned the modeled parameter value of 0.2, noting that the $(\varepsilon + \alpha)$ factor for the scene is given the modeled parameter value of 0.35, and all are dimensionless quantities.

By substitution in (C-4) and definition of terms, we have

$$T'_{CB} = \frac{2.7}{(1.08)(1.25)(1.08)} + \frac{280(1.08 - 1)}{(1.08)(1.25)(1.08)}$$

$$+ \frac{(288)(1.25 - 1)}{(1.25)(1.08)} + \frac{(280)(1.08 - 1)}{(1.08)}$$

$$= 1.85 + 48.01 + 53.33 + 20.74$$

$$= 123.94 \text{ kelvins}$$

where

T_{cos} = Blackbody temperature of the Cosmic Background at microwave wavelengths.

L_{ad} = Loss in the downwelling path, 1.08, a number greater than 1 which expresses a path loss of 0.35 dB.

L_{au} = Loss in the upwelling path, 1.08, a number greater than 1.

T_{ad} = Integrated physical temperature of the downwelling path, 280 kelvins.

T_{au} = Integrated physical temperature of the upwelling path, 280 kelvins.

L_{surf} = Loss in the surface of the cold eddy based on the modeled assumption that $(\varepsilon + \alpha) = 0.2$.

The observing equipment for the sensor is the same as for the detection of the buoy and aircraft carrier:

Collecting area of the antenna (offset, prime-focus antenna configuration with a 30.48-meter-diameter paraboloid)	730 meters^2
Solid-angle main-beam efficiency	0.95
Temperature resolution of receiver	1 kelvin
Thermodynamic temperature of the clutter for the search pattern given in Figure 5 and from Reference [5]	0.45 kelvins

Orthogonal average of temperature resolution of receiver and the clutter temperature	1.1 kelvins
Angle of incidence at 55 degrees latitude	57 degrees
Thermodynamic temperature of the scene as explained by Figures A-3 and A-4	128.87 kelvins
Thermodynamic temperature of the path from the impedance at the phase center of the antenna to the Cosmic Background and including the thermodynamic properties of the cold eddy	123.94 kelvins
Emissivity of the seawater surrounding the cold eddy	0.35
Emissivity of the cold eddy	0.2
Thermometric temperature difference between the surface of the cold eddy and the surrounding seawater	2 kelvins

For a cold eddy whose circular diameter is determined to be 50 kilometers ($A_{ce} = 1.96 \times 10^9$ meters^2) and whose observed location is at 55 degrees latitude, and by substitution of the given parameter values in (C-3), we have

$$\frac{\hat{S}}{C} = \frac{(128.87 - 123.94)[(730)(0.95)][(1.96 \times 10^9)(\cos 57)]}{(38{,}288 \times 10^3)^2 \, (0.008108)^2 \, (1.1)}$$

$$= 34.43, \quad \text{or } 15.37 \text{ dB}$$

When the cold eddy is observed on the equator, and in the plane of the meridian

- The slant range, R_s, to the cold eddy reduces to 35,760 kilometers.
- The term θ_i reduces to zero.
- The term T'_{CB} reduces to 81.82 kelvins by substituting the zenith path attenuation (1.054, a number greater than one, id est, a zenith attenuation of 0.23 dB rather than 0.35 dB at 55 degrees latitude) into Equation (C-4).

By introducing the adjusted numerical values in Equation (C-3) for the observation of the cold eddy at the equator, we obtain

$$\frac{\hat{S}}{C} = 691.6, \quad \text{or} \quad 28.4 \text{ dB}$$

Apparently, the expected value of the S/C ratio increases from 15.37 dB at 55 degrees latitude to 28.4 dB at the equator and in the plane of the meridian--a significant improvement.

The results of the detection of the cold eddy, as they are derived in this appendix, are summarized, with comments, in Section 5.3.

TECHNICAL REPORT STANDARD TITLE PAGE

1. Report No. 86-52	2. Government Accession No.	3. Recipient's Catalog No.
4. Title and Subtitle Geostationary Microwave Imagers Detection Criteria		5. Report Date December 15, 1986 6. Performing Organization Code
7. Author(s) J.M. Stacey		8. Performing Organization Report No.
9. Performing Organization Name and Address JET PROPULSION LABORATORY California Institute of Technology 4800 Oak Grove Drive Pasadena, California 91109		10. Work Unit No. 11. Contract or Grant No. NAS7-918 13. Type of Report and Period Covered External Report JPL Publication
12. Sponsoring Agency Name and Address NATIONAL AERONAUTICS AND SPACE ADMINISTRATION Washington, D.C. 20546		14. Sponsoring Agency Code RE240 BP-414-40-42-10-00

15. Supplementary Notes

16. Abstract

Geostationary orbit is investigated as a vantage point from which to sense remotely the surface features of the planet and its atmosphere--with microwave sensors. The geometrical relationships associated with geostationary altitude are developed to produce an efficient search pattern for the detection of emitting mdeia and metal objects. Power transfer equations are derived from the roots of first principles and explain the expected values of the signal-to-clutter ratios for the detection of aircraft, ships, and buoys and for the detection of natural features where they are manifested as cold and warm eddies. The transport of microwave power is described for modeled detections where the direction of power flow is explained by the Zeroth and Second Laws of Thermodynamics. Mathematical expressions are derived that elucidate the detectability of natural emitting media and metal objects. Signal-to-clutter-ratio comparisons are drawn among detectable objects that show relative detectability with a thermodynamic sensor (microwave receiver) and with a short-pulse radar. These comparisons are modeled with identical antenna structures and at the same operating wavelength. Efficient and practicable antenna concepts are described as they apply to use in geostationary orbit.

17. Key Words (Selected by Author(s))	18. Distribution Statement
Defense; Intelligence; Radar Detection; Astronomy	Unclassified; unlimited

19. Security Classif. (of this report)	20. Security Classif. (of this page)	21. No. of Pages	22. Price
Unclassified	Unclassified		